

CERN-EP-2024-126
13 May 2024

Measurement of the impact-parameter dependent azimuthal anisotropy in coherent ρ^0 photoproduction in Pb–Pb collisions at $\sqrt{s_{NN}} = 5.02$ TeV

ALICE Collaboration*

Abstract

The first measurement of the impact-parameter dependent angular anisotropy in the decay of coherently photoproduced ρ^0 mesons is presented. The ρ^0 mesons are reconstructed through their decay into a pion pair. The measured anisotropy corresponds to the amplitude of the $\cos(2\phi)$ modulation, where ϕ is the angle between the two vectors formed by the sum and the difference of the transverse momenta of the pions, respectively. The measurement was performed by the ALICE Collaboration at the LHC using data from ultraperipheral Pb–Pb collisions at a center-of-mass energy of $\sqrt{s_{NN}} = 5.02$ TeV per nucleon pair. Different impact-parameter regions are selected by classifying the events in nuclear-breakup classes. The amplitude of the $\cos(2\phi)$ modulation is found to increase by about one order of magnitude from large to small impact parameters. Theoretical calculations, which describe the measurement, explain the $\cos(2\phi)$ anisotropy as the result of a quantum interference effect at the femtometer scale that arises from the ambiguity as to which of the nuclei is the source of the photon in the interaction.

© 2024 CERN for the benefit of the ALICE Collaboration.

Reproduction of this article or parts of it is allowed as specified in the CC-BY-4.0 license.

*See Appendix A for the list of collaboration members

1 Introduction

The heavy ions circulating at the Relativistic Heavy-Ion Collider (RHIC) and Large Hadron Collider (LHC) accelerators are accompanied by a strong, Lorentz contracted, electromagnetic field that can be described as a flux of quasi-real photons. This flux makes it possible to study photoproduction interactions at these facilities [1–4]. Most of the experimental work uses ultraperipheral collisions (UPCs) where the colliding ions cross paths at impact parameters larger than the sum of their radii. Given the short range of the strong force, UPCs allow one to separate photon-induced processes from hadronic interactions.

One of the processes that has received great interest is the photonuclear production of a vector meson, where the incoming photon fluctuates into a quark–antiquark color dipole that scatters off the nucleus traveling in the opposite direction (denoted as the target), and appears as a real vector meson. This process can be either coherent, if the photon couples to the nucleus as a whole, or incoherent, if it interacts with a single nucleon. The two processes result in a different transverse momentum (p_T) spectrum; the mean p_T of the vector meson is related to the size of the target in the impact-parameter plane and it is around 60 (500) MeV/ c in the coherent (incoherent) case. In the coherent scenario, it is not known which of the two colliding nuclei emits the photon and which acts as the target, opening up the possibility to study, at femtometer scales, the fundamental quantum mechanical interference between the amplitudes. This idea was first proposed in Ref. [5], where it was noted that interference effects should be stronger: (i) around midrapidity, where the magnitude of both amplitudes is similar, and (ii) at small impact parameters b , where b acts analogously to the distance between slits, in a two-slit interferometer.

Coherent vector meson photoproduction accompanied by electromagnetic dissociation (EMD) offers the opportunity to select different impact parameter regions in UPCs [6]. The electromagnetic field of the heavy ions is so intense that there is a non-negligible probability that the two nuclei, besides interacting to produce the ρ^0 , also exchange photons in an independent EMD interaction, where the excited nuclei emit neutrons at beam rapidities. Experimentally, the emitted neutrons can be detected using two zero-degree calorimeters (ZDCs) each of them covering the direction of one of the incoming colliding nuclei. This allows for classifying UPCs as: (i) $XnXn$, where at least one neutron is detected in each ZDC, (ii) $Xn0n + 0nXn$, where at least one neutron is detected in only one of the ZDCs, and (iii) $0n0n$, where no neutron is detected in the ZDCs; for brevity, the class $Xn0n + 0nXn$ will be denoted as $Xn0n$ in the following text. Since the intensity of the electromagnetic field grows with decreasing impact parameter, the $XnXn$ configuration, where at least three photons are exchanged, selects a region of relatively small impact parameters. The $0nXn$ and $Xn0n$ configurations select a broader impact-parameter range than $XnXn$, while $0n0n$ events encompass all possible impact parameters. EMD is modeled in the RELDIS [7, 8] and \mathbf{n}_0^n [9] models, while the coherent production of vector mesons accompanied by electromagnetic dissociation is studied with \mathbf{n}_0^n and STARlight [10]. According to \mathbf{n}_0^n , the median impact parameter of coherent ρ^0 photoproduction at the LHC energy changes from about 49 fm in $0n0n$ to about 19 fm in $XnXn$.

Ref. [5] proposes the suppression of coherent ρ^0 production at small transverse momentum in UPCs as an observable to study interference effects. This effect was measured by the STAR Collaboration in coherent ρ^0 photoproduction at a center-of-mass energy per nucleon pair of $\sqrt{s_{NN}} = 200$ GeV [11]. The measurement was carried out using two samples, one corresponding to $XnXn$ and the other without any requirement on the detection of neutrons at beam rapidities. As expected, it was observed that the destructive interference was more pronounced in the $XnXn$ sample.

Recently, it was pointed out that the interference can also give rise to an azimuthal anisotropy, since the incoming photons are linearly polarized. It was suggested to look for this effect in the process $\gamma + \gamma \rightarrow l^+ + l^-$ where γ and l^\pm denote photons and leptons, respectively [12]. The dependence of this phenomenon on the impact parameter was studied in Ref. [13]. Shortly thereafter, this effect was mea-

sured, for the XnXn event class, by the STAR Collaboration in Au–Au UPCs at $\sqrt{s_{\text{NN}}} = 200$ GeV [14].

These studies were later extended to the photoproduction of a ρ^0 vector meson, where the ρ^0 inherits the linear polarization of the photon, giving rise to a $\cos(2\phi)$ asymmetry [15, 16]. Here, ϕ is the angle between the two vectors formed by the sum and by the difference of the transverse momenta of the pions produced in the decay $\rho^0 \rightarrow \pi^+\pi^-$. More recently, it was proposed to look for $\cos(\phi)$, $\cos(3\phi)$ [17], and $\cos(4\phi)$ [18] modulations. The first two patterns could be produced by the interference of the production of ρ^0 with QED processes, and the last by the interference of resonant and open production of pion pairs. It was also proposed to search for asymmetries in the photoproduction of a J/ψ vector meson [19]. The predicted $\cos(2\phi)$ modulation was measured by the STAR Collaboration, for ρ^0 coherent production in XnXn events, in Au–Au and U–U UPCs at $\sqrt{s_{\text{NN}}} = 200$ GeV and $\sqrt{s_{\text{NN}}} = 193$ GeV, respectively [20]. This asymmetry was also recently studied by the CMS Collaboration using exclusive diffractive production of jets at the LHC [21].

The ALICE Collaboration has measured the cross section for EMD in Pb–Pb collisions at center-of-mass energies of $\sqrt{s_{\text{NN}}} = 2.76$ TeV [22] and $\sqrt{s_{\text{NN}}} = 5.02$ TeV [23], where a good agreement with the predictions from RELDIS and \mathbf{n}_0^n was found. The ALICE Collaboration has also measured coherent ρ^0 photoproduction in Pb–Pb UPCs at $\sqrt{s_{\text{NN}}} = 2.76$ TeV [24] and $\sqrt{s_{\text{NN}}} = 5.02$ TeV [25], as well as in Xe–Xe UPCs at $\sqrt{s_{\text{NN}}} = 5.44$ TeV [26]. The results were compared to predictions from the STARlight and GDL [27] models in Ref. [24], and from STARlight and \mathbf{n}_0^n in Refs. [25, 26]; in general, the tested models describe well the relative ρ^0 yields in the 0n0n, Xn0n, and XnXn classes. These measurements demonstrate that coherent ρ^0 photoproduction accompanied by EMD is well understood at the LHC and that neutron emission in EMD can be used to select different event classes which are dominated by different impact parameter ranges.

In this Letter, the impact-parameter dependence of the $\cos(2\phi)$ asymmetry is studied in Pb–Pb UPCs at $\sqrt{s_{\text{NN}}} = 5.02$ TeV using the coherent photoproduction of a ρ^0 meson decaying into a pion pair. The measurements are performed at midrapidity in the range $|y| < 0.8$ and in three different EMD classes: 0n0n, Xn0n, and XnXn.

2 Experimental set-up

A full description of the ALICE apparatus and its performance is given in Refs. [28, 29]. A brief description of the sub-detectors involved in this analysis is given hereafter. The ρ^0 meson is detected through its decay into a pion pair at midrapidity, using the Inner Tracking System (ITS) [30] and the Time Projection Chamber (TPC) [31] to reconstruct the pion tracks. The V0 [32] and ALICE Diffractive (AD) [33] detectors, located at forward rapidities, provide a veto, suppressing hadronic interactions. As mentioned in Sec. 1, three different impact-parameter ranges are selected by means of neutrons emitted at forward rapidities, measured by the ZDCs [22].

The ITS is composed of six cylindrical layers coaxial with the beam line. Three different technologies are used, starting from the inner layer: pixels, drift, and strip sensors; each technology is used in two consecutive layers. All six layers are used for tracking, while the two innermost layers, the Silicon Pixel Detector (SPD), are also used for triggering. The TPC is a large cylindrical gaseous detector that surrounds the ITS. It has a central cathode at high voltage and two readout planes at the end caps, composed of multiwire proportional chambers. It is the main tracking detector and provides particle identification (PID) by measuring the specific ionization energy loss. The ITS and the TPC cover a pseudorapidity interval $|\eta| < 0.9$ and the full azimuth; they are located inside a solenoid magnet that provides a magnetic field of $B = 0.5$ T.

The V0 is composed of two scintillator arrays, V0A and V0C, installed on both sides of the nominal interaction point (IP). They cover the pseudorapidity ranges $2.8 < \eta < 5.1$ and $-3.7 < \eta < -1.7$, respec-

tively. The AD consists of two scintillator stations, ADA and ADC, located along the beam line at +16 m and -19 m from the IP and covering the pseudorapidity ranges $4.8 < \eta < 6.3$ and $-7.0 < \eta < -4.9$, respectively.

There are two ZDC detectors for neutrons, ZNA and ZNC, located at ± 112.5 m from the IP along the beam line. They detect neutrons with $|\eta| > 8.8$, with an energy resolution good enough to be sensitive to the emission of a single neutron. Neutron signals are discriminated with a threshold corresponding to an energy deposition of ~ 1 TeV, which is about three standard deviations below the expected signal from a 2.51 TeV neutron. The ZNs also determine the arrival time of the particles, allowing for the rejection of beam-gas interactions involving charge circulating outside the nominal LHC bunch positions.

The analyzed data were recorded by ALICE in 2015, when the LHC provided Pb-Pb collisions at $\sqrt{s_{NN}} = 5.02$ TeV, using a dedicated UPC trigger. This trigger exploits five different signals: four of them veto any activity on either side of the AD or V0 detector within the time window for nominal beam-beam interactions, to suppress hadronic collisions. The fifth signal is a topological trigger that selects events that have at least two track segments, defined as in Ref. [25], in the SPD, with an opening angle in azimuth greater than 153 degrees. This topology was chosen since the coherently produced ρ^0 has a very small transverse momentum and hence the tracks of the pions are almost back-to-back in azimuth. The integrated luminosity of the sample, determined using the V0 detectors as explained in Ref. [25], is about 485 mb^{-1} .

3 Analysis procedure

3.1 Track and event selection

Tracks were required to have a distance of closest approach to the event primary vertex smaller than $0.0182 + 0.0350/(p_T^{\text{trk}})^{1.01}$ cm in the transverse plane and smaller than 2 cm in the longitudinal direction, where p_T^{trk} is the transverse momentum, in GeV/c, associated to the track. Tracks were also required to have more than 50 associated hits in the TPC, to be reconstructed in both ITS and TPC, and to match the track segments in the SPD that fired the trigger.

The events with good tracks were required to fulfill additional selections: (i) have exactly two tracks of opposite sign, (ii) have no offline reconstructed signal in neither the V0 nor AD detectors, and (iii) fulfill the pion selection $n_{\sigma 1}^2 + n_{\sigma 2}^2 < 5^2$, where $n_{\sigma 1}$ ($n_{\sigma 2}$) is the difference, in units of the TPC ionization energy loss resolution, between the measured energy loss for track 1 (track 2) and the expected value for a pion with the same momentum.

Kinematic selections were also applied: (i) the pion pair rapidity lies in the range $|y| < 0.8$ to avoid acceptance edge effects, (ii) the invariant mass of the pion pair is inside the range $0.6 \text{ GeV}/c^2 < m_{\pi\pi} < 0.95 \text{ GeV}/c^2$, and (iii) the transverse momentum of the ρ^0 candidate is less than 0.1 GeV/c to select coherent processes with high purity. With such a selection, the contamination from incoherent events is found to be lower than 4% [25]. More details about event and track selections can be found in Ref. [25].

The data were divided in three independent classes, based on the detection of neutrons at forward rapidity. Events with neutron emission were selected by requiring a signal in ZNA and/or ZNC. The signal time was required to lie within 2 ns from the nominal collision time. As explained in Sec. 1, these classes (0n0n, Xn0n, XnXn) can be used to select different impact-parameter ranges for ultraperipheral collisions. For each neutron class, the data were arranged in seven ϕ intervals of equal size, with ϕ defined as in Sec. 3.2. The efficiency correction (Sec. 3.3) and signal extraction (Sec. 3.4) were then performed separately for each neutron class and ϕ interval.

3.2 Asymmetry angle definition

The anisotropy described in Sec. 1 is predicted to be strongly visible as a function of a variable called ϕ , defined using the momenta of the pions ($\vec{\pi}_{1,2}$) into which the ρ^0 decays. The ϕ angle can be defined in two different ways, which will be referred to as *average* and *charge*, respectively. In both cases ϕ is defined as the angle between the transverse components of \vec{p}_+ and \vec{p}_- , where $\vec{p}_\pm = \vec{\pi}_1 \pm \vec{\pi}_2$. Using the *average* definition, $\vec{\pi}_{1,2}$ are randomly associated to the positive or to the negative track. Using the *charge* definition, $\vec{\pi}_1$ and $\vec{\pi}_2$ are the momenta of the positive and of the negative track, respectively. The *average* definition is helpful since, by construction, it does not allow for a $\cos(\phi)$ component. The two definitions are equivalent in terms of the predicted $\cos(2\phi)$ component. The *average* definition was chosen as the default one, while the *charge* definition was used in the evaluation of the systematic uncertainties. In both cases, the ϕ angle was initially computed within the range of $-\pi$ to π . Then, since $\cos(\phi)$ and $\cos(2\phi)$ are even functions, the resulting values were remapped between 0 and π by flipping the sign of negative values. This procedure improves the stability of signal extraction when fitting the invariant mass spectra in each ϕ interval, by doubling the size of the available sample.

3.3 Corrections

The correction for the acceptance and efficiency of the detector for the reconstruction and selection of the pion tracks, $\text{Acc} \times \varepsilon$, was estimated as a function of the pion pair invariant mass, using the STARlight [10] Monte Carlo (MC) generator and a realistic description of the ALICE apparatus. This MC production describes accurately the raw data on the vector meson kinematics, with the exception of the transverse momentum distribution [24]. In order to improve the agreement of the MC with data, a re-weighting procedure, described in the following, was applied to the generated p_T^2 spectrum. The first step of the procedure is to fit the inclusive pion pair p_T^2 distribution of the generated MC. For sufficiently high transverse momentum, p_T^2 can be approximated with the Mandelstam variable t , while for very low p_T^2 the contribution from the transverse momentum of the photon plays an important role and hence the approximation is no longer valid. Having this in mind, the MC spectrum was fitted for $p_T^2 > (0.01)^2$ (GeV/c)² using the function

$$\frac{dN}{dp_T^2} = c |F(|t|, a_{\text{Pb}}, R_{\text{Pb}})|^2, \quad (1)$$

where c is a normalization constant and $F(|t|)$ is the form factor of the lead nucleus, obtained as a numerical approximation of the Fourier transform of a Wood–Saxon function [34, 35], with fit parameters R_{Pb} and a_{Pb} . The weights were then computed using

$$w(p_T) = \frac{|F(|t|, a_{\text{Pb}}, R_X)|^2}{|F(|t|, a_{\text{Pb}}, R_{\text{Pb}})|^2}, \quad (2)$$

where a_{Pb} is fixed to the fit result and R_X is chosen in such a way that, after applying the weights to each event of a given generated p_T , the reconstructed p_T^2 spectrum in the MC best reproduces the one in the data. This is achieved by minimizing the bin-by-bin difference between the p_T distributions of data and reconstructed MC as a function of R_X , using a χ^2 -like variable, in the region $p_T^2 > (0.01)^2$ (GeV/c)², where the model used for the reweighting is valid. It was verified that the best-fit values of R_X computed for different ϕ ranges were all compatible among themselves, hence the weights were obtained utilizing the full data set.

The $\text{Acc} \times \varepsilon$ correction was obtained using the re-weighted STARlight MC simulations by computing the ratio of reconstructed to generated number of pion pairs in each invariant mass and ϕ interval, after applying the weights discussed above at the generation level. The number of pion pairs found in data, for each invariant mass and ϕ interval, was then divided by $\text{Acc} \times \varepsilon$, to obtain the corrected mass spectra. This was done for each neutron class and ϕ range. The integrated $\text{Acc} \times \varepsilon$ was found to slightly increase

as a function of the invariant mass, ranging from $\sim 10.5\%$ at $m_{\pi\pi} = 0.6 \text{ GeV}/c^2$ to $\sim 14\%$ at $m_{\pi\pi} = 0.95 \text{ GeV}/c^2$.

3.4 Signal extraction

The corrected invariant mass spectra, in each neutron class and in each ϕ interval, were fitted with:

$$\frac{dN}{dm_{\pi\pi}} = P(m_{\pi\pi}) + n_{\mu\mu} M(m_{\pi\pi}), \quad (3)$$

where $m_{\pi\pi}$ is the pion pair invariant mass, $P(m_{\pi\pi})$ is the function used to describe the pion pair spectrum, $M(m_{\pi\pi})$ is the shape, estimated with a dedicated MC based on the STARlight generator, of the background originating from muons produced in the $\gamma\gamma \rightarrow \mu^+\mu^-$ process and misidentified as pions, and $n_{\mu\mu}$ is a normalization constant for said background. Two different parameterizations were used for the pion spectrum. The first parameterization uses a modified Söding model [36]:

$$P(m_{\pi\pi}) = |A \cdot BW_\rho + B|^2, \quad (4)$$

where BW_ρ is the relativistic Breit–Wigner shape that describes the ρ^0 , A is its amplitude, and B is the amplitude of the continuum pion pair production. The relativistic Breit–Wigner function describing the ρ^0 resonance is:

$$BW_\rho = \frac{\sqrt{m_{\pi\pi} m_\rho \Gamma_\rho(m_{\pi\pi})}}{m_{\pi\pi}^2 - m_\rho^2 + i m_\rho \Gamma_\rho(m_{\pi\pi})}, \quad (5)$$

where m_ρ is the ρ^0 pole mass and

$$\Gamma_\rho(m_{\pi\pi}) = \Gamma(m_\rho) \frac{m_\rho}{m_{\pi\pi}} \left(\frac{m_{\pi\pi}^2 - 4m_\pi^2}{m_\rho^2 - 4m_\pi^2} \right)^{3/2}, \quad (6)$$

where $\Gamma(m_\rho)$ is the ρ^0 pole width. Since BW_ρ is complex, an interference term between the ρ^0 and the continuum arises from the square module in Eq. (4). The second parameterization uses the model by Ross and Stodolsky [37]:

$$P(m_{\pi\pi}) = f |BW_\rho|^2 \left(\frac{m_\rho}{m_{\pi\pi}} \right)^k, \quad (7)$$

with fit parameters f and k .

The fits were performed by fixing m_ρ and $\Gamma(m_\rho)$ to the central values reported for a ρ^0 formed in a photoproduction reaction, namely, $m_\rho = 769.2 \text{ MeV}/c^2$ and $\Gamma(m_\rho) = 151.5 \text{ MeV}/c^2$ [38]. As discussed in Ref. [25], it was verified that the extracted ρ^0 yield does not vary significantly when the fit function is modified to include a contribution from ω decays.

In order to assess the stability of the signal extraction, the latter was carried out, for each ϕ interval, with 48 different strategies, obtained by: employing 12 different combinations of bin size and fit range (the widest tested range being $0.6\text{-}0.95 \text{ GeV}/c^2$ and the narrowest $0.65\text{-}0.9 \text{ GeV}/c^2$), using the Söding or the Ross-Stodolsky model to describe the pion pair mass spectrum, and using $n_{\mu\mu}$ as a free fit parameter or fixing it to zero. An example of the mass fits, for a specific ϕ interval and for the 0n0n and XnXn classes, is shown in Fig. 1. After the fit, the ρ^0 yield is obtained by integrating the signal function, $|ABW_\rho|^2$ for the Söding model and $f|BW_\rho|^2$ for the Ross-Stodolsky model, in the mass range $0.6 < m_{\pi\pi} \text{ (GeV}/c^2) < 0.95$. Such a range was chosen to be consistent with the STAR measurement [20] and with available theory calculations (see Sec. 4 for details).

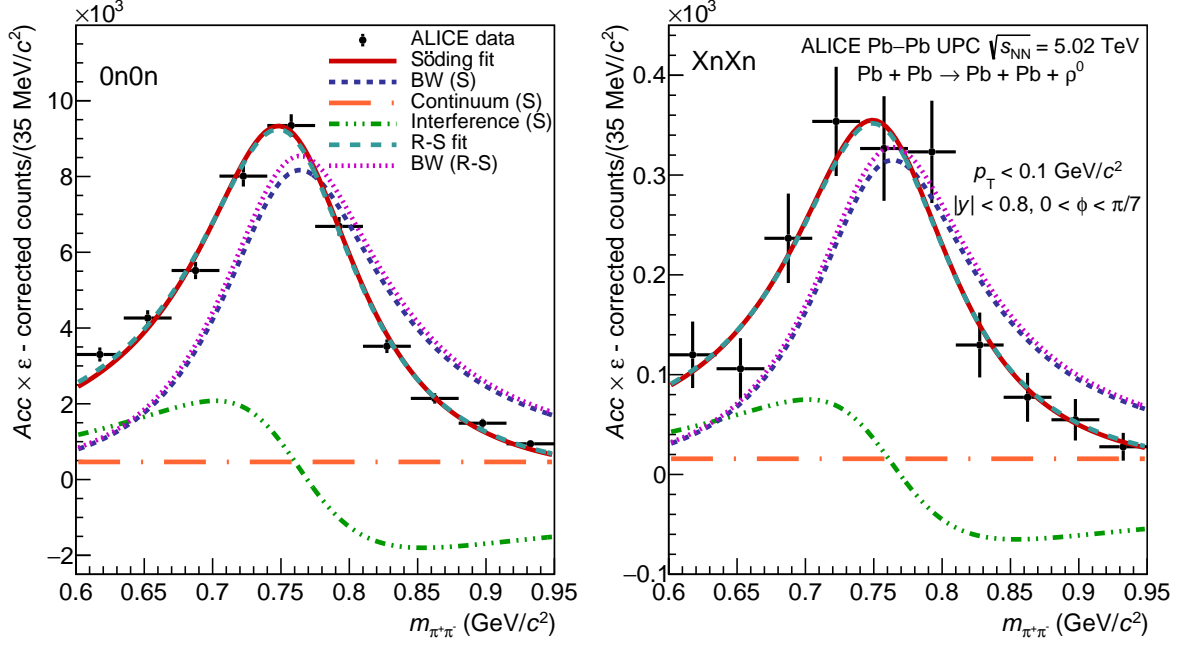


Figure 1: Invariant-mass distribution of pion pairs, with superimposed Söding (solid line) and Ross-Stodolsky (dotted line) fits, for the range $0 < \phi < \pi/7$ in the 0n0n (left) and XnXn (right) neutron classes. The different components of the pion-pair production amplitude in the Söding model are shown: the Breit–Wigner shape that describes the ρ^0 (finer dotted line), the continuum process (dash-dotted line), and the interference between the ρ^0 and the continuum (dash-dot-dot-dot line). The Breit–Wigner extracted from the Ross-Stodolsky model (finest dotted line) is also shown. In this example, the background contribution from misidentified muons is fixed to zero in the fit.

3.5 Asymmetry extraction

The extraction of the amplitude of the modulation is affected by the migration of events between neutron classes, due to ZDC detector efficiency and pile-up effects, as discussed in Ref. [25]. To take this into account, a simultaneous fit to the measured ρ^0 yield as a function of ϕ in all three experimental classes (0n0n, Xn0n, XnXn) was performed, using the following expression:

$$\begin{pmatrix} n_{\rho\ 0n0n}(\phi) \\ n_{\rho\ Xn0n}(\phi) \\ n_{\rho\ XnXn}(\phi) \end{pmatrix} = \begin{pmatrix} 1 \\ 1 \\ 1 \end{pmatrix} + \begin{pmatrix} w_{0n0n \rightarrow 0n0n} & w_{Xn0n \rightarrow 0n0n} & w_{XnXn \rightarrow 0n0n} \\ w_{0n0n \rightarrow Xn0n} & w_{Xn0n \rightarrow Xn0n} & w_{XnXn \rightarrow Xn0n} \\ w_{0n0n \rightarrow XnXn} & w_{Xn0n \rightarrow XnXn} & w_{XnXn \rightarrow XnXn} \end{pmatrix} \begin{pmatrix} a_{2\ 0n0n} \\ a_{2\ Xn0n} \\ a_{2\ XnXn} \end{pmatrix} \cos(2\phi), \quad (8)$$

where $n_{\rho\ 0n0n}$ is the normalized ρ^0 yield in a given ϕ range for the experimental 0n0n class, and similarly for other classes, and the fitting parameters $a_{2\ 0n0n}$, $a_{2\ Xn0n}$, and $a_{2\ XnXn}$ are the amplitudes of the $\cos(2\phi)$ modulation in the corresponding three physical classes. The coefficients $w_{Y \rightarrow Z}$ represent the contribution of the physical neutron class Y to the yield in the experimental neutron class Z, computed using the measured cross-section ratios and migration probabilities as determined in Ref. [25]. The constant term is fixed to unity by normalization. An example of this simultaneous fit is shown in Fig. 2.

The central value and the statistical uncertainty of the $\cos(2\phi)$ modulation amplitude were determined, for each neutron emission class, by averaging the results obtained with the 48 fit configurations described in Sec. 3.4.

3.6 Systematic uncertainties

The systematic uncertainty related to the signal extraction includes the effect on the extracted $\cos(2\phi)$ amplitudes of variations in the strategy for fitting the invariant mass spectra. These include: binning,

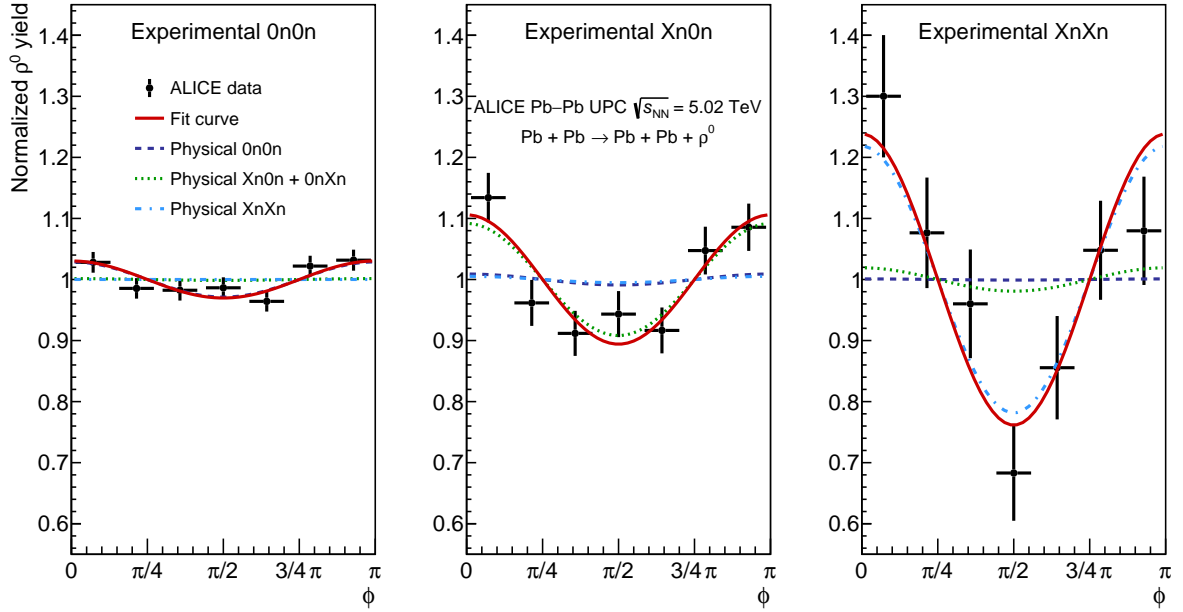


Figure 2: Example of a simultaneous fit to the ρ^0 yield as a function of ϕ , used to extract the amplitude of the $\cos(2\phi)$ modulation in all neutron classes. The contribution of each physical class to the yield in all experimental classes is shown.

range, modeling of the ρ^0 signal, and treatment of background. The uncertainty was obtained as the standard deviation of the distribution of the fitted amplitudes over the 48 trials mentioned in Sec. 3.4. This uncertainty is 12% for 0n0n, 9% for Xn0n, and 13% for XnXn.

An additional systematic uncertainty, related to the definition of the ϕ angle, was estimated by testing two variations in the analysis strategy. In the first variation, ϕ is computed according to the *charge* definition mentioned in Sec. 3.2. In this case, the yield distribution can have a sizeable $\cos(\phi)$ component [17], which is added to the fit function of Eq. (8), with its amplitude as an additional free parameter. In the second variation, the *average* definition of ϕ is used, as in the default strategy, but a $\cos(\phi)$ component is nevertheless added to the fit function. The systematic uncertainty was evaluated in each class as the largest difference between the result obtained with the default setting and that obtained with the two strategies presented in this paragraph. It amounts to 3.6% for 0n0n, 5.6% for Xn0n, and 3.3% for XnXn.

As a consistency check for the $\text{Acc} \times \varepsilon$ correction, the analysis was repeated in several rapidity sub-ranges, each containing approximately half the total number of reconstructed ρ^0 candidates. In each neutron emission class, the amplitudes extracted in sub-ranges were all found to be compatible, within one standard deviation, with each other and with the amplitude extracted in the full rapidity range. The uncertainty on the $\text{Acc} \times \varepsilon$ correction arises then mainly from the re-weighting procedure described in Sec. 3.3. It was obtained by using the two values of R_X for which the χ^2 increases by one unit with respect to the minimum, instead of the R_X value that minimizes the χ^2 . The systematic uncertainty is estimated in each class as the largest difference between the results obtained with the original and with the modified sets of weights. It amounts to 2.9% for 0n0n, 0.8% for Xn0n, and 0.9% for XnXn.

The systematic uncertainties related to the migration of events across neutron classes are evaluated by propagating the uncertainties of the ZN pile-up probability (9%) and efficiency (1%), all taken from Ref [25], to the extraction of the $\cos(2\phi)$ amplitude. The resulting uncertainty from pile-up is 0.1%, 2.3%, and 0.9%, respectively, for the 0n0n, Xn0n, and XnXn classes. The uncertainty from the ZN efficiency is 0.7%, 0.1%, and 0.1%, respectively, for the 0n0n, Xn0n, and XnXn classes.

The contributions to the systematic uncertainty on the amplitude of the $\cos(2\phi)$ modulation discussed in

the previous paragraphs are listed in Table 1. The total uncertainty is obtained as the quadratic sum of all the contributions. It amounts to 12.6% for 0n0n, 11% for Xn0n, and 13.3% for XnXn, and is dominated by the signal extraction for all event classes.

Table 1: Summary of the relative systematic uncertainties for the measured amplitude of the $\cos(2\phi)$ modulation.

Source	Uncertainty (%)		
	0n0n	Xn0n + 0nXn	XnXn
Signal extraction	12	9.1	13
ϕ definition	3.6	5.7	3.3
$\text{Acc} \times \varepsilon$	2.9	0.8	0.9
ZN pile-up	0.1	2.3	0.9
ZN efficiency	0.7	0.1	0.1
Total	12.6	11.0	13.3

4 Results

Figure 3 shows the extracted amplitude of the $\cos(2\phi)$ modulation as a function of the neutron class; the numerical values are reported in Table 2, along with the \mathbf{n}_0^n MC estimates of the median impact parameter of the collision for each neutron class. Similar values for the median impact parameters are found using the analytical model presented in Ref. [39]; the values for the XnXn case are also similar to those reported in Ref. [6]. The table also reports the amplitudes predicted by two models described below. The measured anisotropy shows a clear trend with the impact parameter, with a significant increase, by one order of magnitude, from 0n0n to XnXn.

The results are compared with the model by H. Xing *et al.* [15]. In this model, the quasi-real photon exchanged by the nuclei is treated as a color quark–antiquark dipole, that recombines to produce a ρ^0 after scattering off the color-glass-condensate state [40] inside the nuclei. As discussed in Sec. 1, the $\cos(2\phi)$ anisotropy in the model emerges from the presence of two elements: the first is that the photon is linearly polarized along the impact parameter and this polarization is transferred to the produced vector meson; the second is that there is an interference between the two amplitudes that contribute to the cross section of the vector meson photoproduction process. The interference effect increases as the impact parameter decreases, producing a larger anisotropy for small impact parameters. The uncertainty of the model mostly comes from the probability of emitting a neutron from the scattered nucleus at a given impact parameter, where the latter has been estimated using three different parametrizations from Refs. [41–43]. The model prediction is compatible with data for all neutron classes. The measured amplitudes are also compared to the model of W. Zhao *et al.* [44], which is based on the same formalism as the model by H. Xing *et al.* [15] with two main differences: (i) the interaction of the quark–antiquark dipole with the target is implemented by computing the corresponding Wilson lines, and (ii) the color-charge density used to obtain the Wilson lines is varied event-by-event to represent the different possible color configurations of the target. The quoted uncertainty in the model originates from the statistical precision related to the finite number of sampled configurations. This model, which predicts a milder variation of the modulation amplitude with the neutron class as compared to Xing *et al.*, also gives a reasonable description of the data, with the possible exception of the 0n0n class.

For the XnXn class, the amplitude measured by ALICE is also compared with the ones [20] measured by the STAR Collaboration for Au–Au and U–U collisions at the center-of-mass energies of $\sqrt{s_{\text{NN}}} = 200$ GeV and $\sqrt{s_{\text{NN}}} = 193$ GeV, respectively. It is found to be compatible with both. This is consistent with the models, which, for the XnXn selection, predict the $\cos(2\phi)$ modulation amplitude

to vary with the colliding nuclei and the center-of-mass energy by less than the current experimental uncertainties.

Table 2: Amplitudes of the $\cos(2\phi)$ modulation of the ρ^0 yield as a function of ϕ in all neutron classes, with statistical and systematic uncertainties. An estimate of the median impact parameter of the collision in each neutron class, obtained with the \mathbf{n}_0^n MC, is also reported, as well as the predictions by the H. Xing *et al.* [15] and W. Zhao *et al.* [44] models.

Neutron class	median b (\mathbf{n}_0^n)	amplitude	stat.	syst.	H. Xing <i>et al.</i>	W. Zhao <i>et al.</i>
0n0n	49.0 fm	0.028	0.011	0.003	0.015 – 0.031	0.042 – 0.044
Xn0n	22.5 fm	0.14	0.04	0.016	0.14 – 0.19	0.136 – 0.138
XnXn	18.2 fm	0.25	0.06	0.03	0.26 – 0.29	0.200 – 0.214

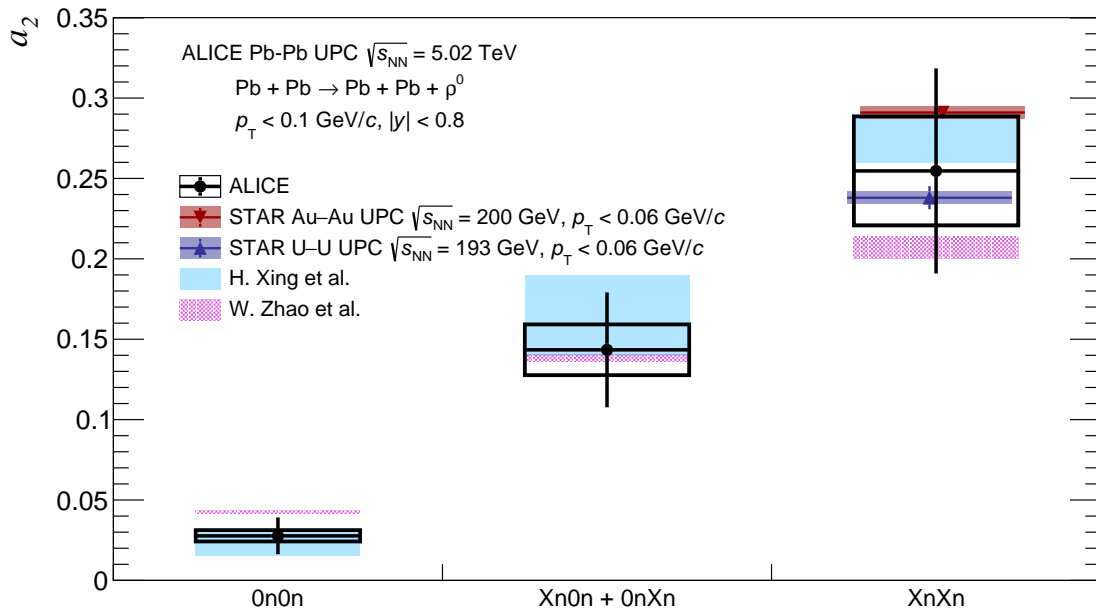


Figure 3: Amplitudes of the $\cos(2\phi)$ modulation of the ρ^0 yield in Pb–Pb collisions at $\sqrt{s_{\text{NN}}} = 5.02$ TeV in all neutron classes. The results are compared with the Xing *et al.* [15] and W. Zhao *et al.* [44] model predictions and, for the XnXn class, with the STAR results [20] in Au–Au and U–U collisions at RHIC. For all the experimental data points, statistical uncertainties are represented with a bar and systematic uncertainties with a box.

5 Summary

The first measurement of the impact-parameter dependent angular anisotropy in the pion-pair decay of coherently photoproduced ρ^0 mesons from Pb–Pb ultraperipheral collisions at a center-of-mass energy of $\sqrt{s_{\text{NN}}} = 5.02$ TeV, performed with the ALICE detector, has been presented. The anisotropy is quantified via the distribution of the azimuthal angle ϕ , defined in Sec. 3.2. The impact parameter is estimated considering neutron emission at forward rapidity. A significant, impact-parameter dependent, $\cos(2\phi)$ modulation is observed, with the amplitude of the modulation increasing by about one order of magnitude from the 0n0n (no neutrons emitted, large impact parameter) to the XnXn (neutrons emitted by both colliding nuclei, relatively small impact parameter) class. This trend is reproduced by the theoretical models [15, 44]. The result for the XnXn class is compatible with similar measurements by the STAR Collaboration.

The coherent photonuclear production of a vector meson in UPCs can be seen as a double-slit experiment [45], where the interference occurs between the amplitudes for quasi-real photon emission by either of the two colliding nuclei. The unambiguous observation of this interference through the measurement of the $\cos(2\phi)$ anisotropy of the ρ^0 yield is a proof of the validity of quantum mechanics at femtometer scales. This is the first measurement of this effect in terms of the impact-parameter dependence. The larger data samples expected from the LHC Run 3 and Run 4 will enable a detailed characterization of the quantum interference effects.

Acknowledgements

The ALICE Collaboration would like to thank all its engineers and technicians for their invaluable contributions to the construction of the experiment and the CERN accelerator teams for the outstanding performance of the LHC complex. The ALICE Collaboration gratefully acknowledges the resources and support provided by all Grid centres and the Worldwide LHC Computing Grid (WLCG) collaboration. The ALICE Collaboration acknowledges the following funding agencies for their support in building and running the ALICE detector: A. I. Alikhanyan National Science Laboratory (Yerevan Physics Institute) Foundation (ANSL), State Committee of Science and World Federation of Scientists (WFS), Armenia; Austrian Academy of Sciences, Austrian Science Fund (FWF): [M 2467-N36] and Nationalstiftung für Forschung, Technologie und Entwicklung, Austria; Ministry of Communications and High Technologies, National Nuclear Research Center, Azerbaijan; Conselho Nacional de Desenvolvimento Científico e Tecnológico (CNPq), Financiadora de Estudos e Projetos (Finep), Fundação de Amparo à Pesquisa do Estado de São Paulo (FAPESP) and Universidade Federal do Rio Grande do Sul (UFRGS), Brazil; Bulgarian Ministry of Education and Science, within the National Roadmap for Research Infrastructures 2020-2027 (object CERN), Bulgaria; Ministry of Education of China (MOEC), Ministry of Science & Technology of China (MSTC) and National Natural Science Foundation of China (NSFC), China; Ministry of Science and Education and Croatian Science Foundation, Croatia; Centro de Aplicaciones Tecnológicas y Desarrollo Nuclear (CEADEN), Cubaenergía, Cuba; Ministry of Education, Youth and Sports of the Czech Republic, Czech Republic; The Danish Council for Independent Research | Natural Sciences, the VILLUM FONDEN and Danish National Research Foundation (DNRF), Denmark; Helsinki Institute of Physics (HIP), Finland; Commissariat à l’Energie Atomique (CEA) and Institut National de Physique Nucléaire et de Physique des Particules (IN2P3) and Centre National de la Recherche Scientifique (CNRS), France; Bundesministerium für Bildung und Forschung (BMBF) and GSI Helmholtzzentrum für Schwerionenforschung GmbH, Germany; General Secretariat for Research and Technology, Ministry of Education, Research and Religions, Greece; National Research, Development and Innovation Office, Hungary; Department of Atomic Energy Government of India (DAE), Department of Science and Technology, Government of India (DST), University Grants Commission, Government of India (UGC) and Council of Scientific and Industrial Research (CSIR), India; National Research and Innovation Agency - BRIN, Indonesia; Istituto Nazionale di Fisica Nucleare (INFN), Italy; Japanese Ministry of Education, Culture, Sports, Science and Technology (MEXT) and Japan Society for the Promotion of Science (JSPS) KAKENHI, Japan; Consejo Nacional de Ciencia (CONACYT) y Tecnología, through Fondo de Cooperación Internacional en Ciencia y Tecnología (FONCICYT) and Dirección General de Asuntos del Personal Académico (DGAPA), Mexico; Nederlandse Organisatie voor Wetenschappelijk Onderzoek (NWO), Netherlands; The Research Council of Norway, Norway; Pontificia Universidad Católica del Perú, Peru; Ministry of Science and Higher Education, National Science Centre and WUT ID-UB, Poland; Korea Institute of Science and Technology Information and National Research Foundation of Korea (NRF), Republic of Korea; Ministry of Education and Scientific Research, Institute of Atomic Physics, Ministry of Research and Innovation and Institute of Atomic Physics and Universitatea Nationala de Stiinta si Tehnologie Politehnica Bucuresti, Romania; Ministry of Education, Science, Research and Sport of the Slovak Republic, Slovakia; National Research Foundation of South Africa, South Africa; Swedish Research Council (VR) and Knut & Alice Wallenberg Founda-

tion (KAW), Sweden; European Organization for Nuclear Research, Switzerland; Suranaree University of Technology (SUT), National Science and Technology Development Agency (NSTDA) and National Science, Research and Innovation Fund (NSRF via PMU-B B05F650021), Thailand; Turkish Energy, Nuclear and Mineral Research Agency (TENMAK), Turkey; National Academy of Sciences of Ukraine, Ukraine; Science and Technology Facilities Council (STFC), United Kingdom; National Science Foundation of the United States of America (NSF) and United States Department of Energy, Office of Nuclear Physics (DOE NP), United States of America. In addition, individual groups or members have received support from: Czech Science Foundation (grant no. 23-07499S), Czech Republic; European Research Council (grant no. 950692), European Union; ICSC - Centro Nazionale di Ricerca in High Performance Computing, Big Data and Quantum Computing, European Union - NextGenerationEU; Academy of Finland (Center of Excellence in Quark Matter) (grant nos. 346327, 346328), Finland.

References

- [1] G. Baur, K. Hencken, D. Trautmann, S. Sadovsky, and Y. Kharlov, “Coherent $\gamma\gamma$ and γA interactions in very peripheral collisions at relativistic ion colliders”, *Phys.Rep.* **364** (2002) 359–450, arXiv:hep-ph/0112211 [hep-ph].
- [2] A. J. Baltz *et al.*, “The Physics of Ultraperipheral Collisions at the LHC”, *Phys. Rep.* **458** (2008) 1–171, arXiv:0706.3356 [nucl-ex].
- [3] J. G. Contreras and J. D. Tapia Takaki, “Ultra-peripheral heavy-ion collisions at the LHC”, *Int. J. Mod. Phys. A* **30** (2015) 1542012.
- [4] S. R. Klein and H. Mäntysaari, “Imaging the nucleus with high-energy photons”, *Nature Rev. Phys.* **1** (2019) 662–674, arXiv:1910.10858 [hep-ex].
- [5] S. R. Klein and J. Nystrand, “Interference in exclusive vector meson production in heavy ion collisions”, *Phys. Rev. Lett.* **84** (2000) 2330–2333, arXiv:hep-ph/9909237.
- [6] A. J. Baltz, S. R. Klein, and J. Nystrand, “Coherent vector meson photoproduction with nuclear breakup in relativistic heavy ion collisions”, *Phys. Rev. Lett.* **89** (2002) 012301, arXiv:nucl-th/0205031.
- [7] I. A. Pshenichnov, J. P. Bondorf, I. N. Mishustin, A. Ventura, and S. Masetti, “Mutual heavy ion dissociation in peripheral collisions at ultrarelativistic energies”, *Phys. Rev. C* **64** (2001) 024903, arXiv:nucl-th/0101035.
- [8] I. A. Pshenichnov, “Electromagnetic excitation and fragmentation of ultrarelativistic nuclei”, *Phys. Part. Nucl.* **42** (2011) 215–250.
- [9] M. Broz, J. G. Contreras, and J. D. Tapia Takaki, “A generator of forward neutrons for ultra-peripheral collisions: n_0^n ”, *Comput. Phys. Commun.* (2020) 107181, arXiv:1908.08263 [nucl-th].
- [10] S. R. Klein, J. Nystrand, J. Seger, Y. Gorbunov, and J. Butterworth, “STARlight: A Monte Carlo simulation program for ultra-peripheral collisions of relativistic ions”, *Comput. Phys. Commun.* **212** (2017) 258–268, arXiv:1607.03838 [hep-ph].
- [11] **STAR** Collaboration, B. I. Abelev *et al.*, “Observation of Two-source Interference in the Photoproduction Reaction $Au Au \rightarrow Au Au \rho^0$ ”, *Phys. Rev. Lett.* **102** (2009) 112301, arXiv:0812.1063 [nucl-ex].
- [12] C. Li, J. Zhou, and Y.-J. Zhou, “Probing the linear polarization of photons in ultraperipheral heavy ion collisions”, *Phys. Lett. B* **795** (2019) 576–580, arXiv:1903.10084 [hep-ph].

- [13] C. Li, J. Zhou, and Y.-J. Zhou, “Impact parameter dependence of the azimuthal asymmetry in lepton pair production in heavy ion collisions”, *Phys. Rev. D* **101** (2020) 034015, arXiv:1911.00237 [hep-ph].
- [14] **STAR** Collaboration, J. Adam *et al.*, “Measurement of e^+e^- Momentum and Angular Distributions from Linearly Polarized Photon Collisions”, *Phys. Rev. Lett.* **127** (2021) 052302, arXiv:1910.12400 [nucl-ex].
- [15] H. Xing, C. Zhang, J. Zhou, and Y.-J. Zhou, “The $\cos 2\phi$ azimuthal asymmetry in ρ^0 meson production in ultraperipheral heavy ion collisions”, *JHEP* **10** (2020) 064, arXiv:2006.06206 [hep-ph].
- [16] W. Zha, J. D. Brandenburg, L. Ruan, Z. Tang, and Z. Xu, “Exploring the double-slit interference with linearly polarized photons”, *Phys. Rev. D* **103** (2021) 033007, arXiv:2006.12099 [hep-ph].
- [17] Y. Hagiwara, C. Zhang, J. Zhou, and Y.-J. Zhou, “Coulomb nuclear interference effect in dipion production in ultraperipheral heavy ion collisions”, *Phys. Rev. D* **103** (2021) 074013, arXiv:2011.13151 [hep-ph].
- [18] Y. Hagiwara, C. Zhang, J. Zhou, and Y.-J. Zhou, “Probing the gluon tomography in photoproduction of dipion”, *Phys. Rev. D* **104** (2021) 094021, arXiv:2106.13466 [hep-ph].
- [19] J. D. Brandenburg, Z. Xu, W. Zha, C. Zhang, J. Zhou, and Y. Zhou, “Exploring gluon tomography with polarization dependent diffractive J/ψ production”, *Phys. Rev. D* **106** (2022) 074008, arXiv:2207.02478 [hep-ph].
- [20] **STAR** Collaboration, M. Abdallah *et al.*, “Tomography of ultrarelativistic nuclei with polarized photon-gluon collisions”, *Sci. Adv.* **9** (2023) eabq3903, arXiv:2204.01625 [nucl-ex].
- [21] **CMS** Collaboration, A. Tumasyan *et al.*, “Azimuthal Correlations within Exclusive Dijets with Large Momentum Transfer in Photon-Lead Collisions”, *Phys. Rev. Lett.* **131** (2023) 051901, arXiv:2205.00045 [nucl-ex].
- [22] **ALICE** Collaboration, B. Abelev *et al.*, “Measurement of the Cross Section for Electromagnetic Dissociation with Neutron Emission in Pb–Pb Collisions at $\sqrt{s_{NN}} = 2.76$ TeV”, *Phys. Rev. Lett.* **109** (2012) 252302, arXiv:1203.2436 [nucl-ex].
- [23] **ALICE** Collaboration, S. Acharya *et al.*, “Neutron emission in ultraperipheral Pb–Pb collisions at $\sqrt{s_{NN}} = 5.02$ TeV”, *Phys. Rev. C* **107** (2023) 064902, arXiv:2209.04250 [nucl-ex].
- [24] **ALICE** Collaboration, J. Adam *et al.*, “Coherent ρ^0 photoproduction in ultra-peripheral Pb–Pb collisions at $\sqrt{s_{NN}} = 2.76$ TeV”, *JHEP* **09** (2015) 095, arXiv:1503.09177 [nucl-ex].
- [25] **ALICE** Collaboration, S. Acharya *et al.*, “Coherent photoproduction of ρ^0 vector mesons in ultra-peripheral Pb–Pb collisions at $\sqrt{s_{NN}} = 5.02$ TeV”, *JHEP* **06** (2020) 035, arXiv:2002.10897 [nucl-ex].
- [26] **ALICE** Collaboration, S. Acharya *et al.*, “First measurement of coherent ρ^0 photoproduction in ultra-peripheral Xe–Xe collisions at $\sqrt{s_{NN}} = 5.44$ TeV”, *Phys. Lett. B* **820** (2021) 136481, arXiv:2101.02581 [nucl-ex].
- [27] V. Rebyakova, M. Strikman, and M. Zhalov, “Coherent ρ and J/ψ photoproduction in ultraperipheral processes with electromagnetic dissociation of heavy ions at RHIC and LHC”, *Phys. Lett. B* **710** (2012) 647–653, arXiv:1109.0737 [hep-ph].

- [28] **ALICE** Collaboration, K. Aamodt *et al.*, “The ALICE experiment at the CERN LHC”, *JINST* **3** (2008) S08002.
- [29] **ALICE** Collaboration, B. Abelev *et al.*, “Performance of the ALICE Experiment at the CERN LHC”, *Int. J. Mod. Phys. A* **29** (2014) 1430044, arXiv:1402.4476 [nucl-ex].
- [30] **ALICE** Collaboration, K. Aamodt *et al.*, “Alignment of the ALICE Inner Tracking System with cosmic-ray tracks”, *JINST* **5** (2010) P03003, arXiv:1001.0502 [physics.ins-det].
- [31] J. Alme *et al.*, “The ALICE TPC, a large 3-dimensional tracking device with fast readout for ultra-high multiplicity events”, *Nucl. Instrum. Meth. A* **622** (2010) 316–367, arXiv:1001.1950 [physics.ins-det].
- [32] **ALICE** Collaboration, E. Abbas *et al.*, “Performance of the ALICE VZERO system”, *JINST* **8** (2013) P10016, arXiv:1306.3130 [nucl-ex].
- [33] **LHC Forward Physics Working Group** Collaboration, K. Akiba *et al.*, “LHC Forward Physics”, *J. Phys. G Nucl. Part* **43** (2016) 110201, arXiv:1611.05079 [hep-ph].
- [34] S. R. Klein and J. Nystrand, “Exclusive vector meson production in relativistic heavy ion collisions”, *Phys. Rev. C* **60** (1999) 014903, arXiv:hep-ph/9902259 [hep-ph].
- [35] L. C. Maximon and R. A. Schrack, “The form factor of the Fermi model spatial distribution”, *J. Res. Natl. Bur. Stand. B* **70** (1966) 85–94.
- [36] A. S. Krass, “Interference Effects in Photoproduction of ρ^0 Mesons”, *Phys. Rev.* **159** (1967) 1496–1500.
- [37] M. Ross and L. Stodolsky, “Photon Dissociation Model for Vector-Meson Photoproduction”, *Phys. Rev.* **149** (1966) 1172–1181.
- [38] **Particle Data Group** Collaboration, R. L. Workman *et al.*, “Review of Particle Physics”, *PTEP* **2022** (2022) 083C01.
- [39] G. Baur, K. Hencken, A. Aste, D. Trautmann, and S. R. Klein, “Multiphoton exchange processes in ultraperipheral relativistic heavy ion collisions”, *Nucl. Phys. A* **729** (2003) 787–808, arXiv:nucl-th/0307031.
- [40] F. Gelis, E. Iancu, J. Jalilian-Marian, and R. Venugopalan, “The Color Glass Condensate”, *Ann. Rev. Nucl. Part. Sci.* **60** (2010) 463–489, arXiv:1002.0333 [hep-ph].
- [41] C. A. Bertulani and G. Baur, “Electromagnetic Processes in Relativistic Heavy Ion Collisions”, *Phys. Rep.* **163** (1988) 299.
- [42] A. J. Baltz, M. J. Rhoades-Brown, and J. Weneser, “Heavy ion partial beam lifetimes due to Coulomb induced processes”, *Phys. Rev. E* **54** (1996) 4233–4239.
- [43] A. J. Baltz and M. Strikman, “Suppression of heavy ion $\gamma\gamma$ production of the Higgs particle by Coulomb dissociation”, *Phys. Rev. D* **57** (1998) 548–549, arXiv:hep-ph/9705220.
- [44] H. Mäntysaari, F. Salazar, B. Schenke, C. Shen, and W. Zhao, “Effects of nuclear structure and quantum interference on diffractive vector meson production in ultraperipheral nuclear collisions”, *Phys. Rev. C* **109** (2024) 024908, arXiv:2310.15300 [nucl-th].
- [45] J. Nystrand, A. J. Baltz, and S. R. Klein, “Aspects of Coulomb dissociation and interference in peripheral nucleus-nucleus collisions”, in *Workshop on Electromagnetic Probes of Fundamental Physics*, pp. 161–170. 3, 2002. arXiv:nucl-th/0203062.

A The ALICE Collaboration

S. Acharya¹²⁷, D. Adamová⁸⁶, A. Agarwal¹³⁵, G. Aglieri Rinella³², L. Aglietta²⁴, M. Agnello²⁹, N. Agrawal²⁵, Z. Ahammed¹³⁵, S. Ahmad¹⁵, S.U. Ahn⁷¹, I. Ahuja³⁷, A. Akindinov¹⁴¹, V. Akishina³⁸, M. Al-Turany⁹⁷, D. Aleksandrov¹⁴¹, B. Alessandro⁵⁶, H.M. Alfanda⁶, R. Alfaro Molina⁶⁷, B. Ali¹⁵, A. Alici²⁵, N. Alizadehvandchali¹¹⁶, A. Alkin¹⁰⁴, J. Alme²⁰, G. Alocco⁵², T. Alt⁶⁴, A.R. Altamura⁵⁰, I. Altsybeev⁹⁵, J.R. Alvarado⁴⁴, M.N. Anaam⁶, C. Andrei⁴⁵, N. Andreou¹¹⁵, A. Andronic¹²⁶, E. Andronov¹⁴¹, V. Anguelov⁹⁴, F. Antinori⁵⁴, P. Antonioli⁵¹, N. Apadula⁷⁴, L. Aphecetche¹⁰³, H. Appelshäuser⁶⁴, C. Arata⁷³, S. Arcelli²⁵, M. Aresti²², R. Arnaldi⁵⁶, J.G.M.C.A. Arneiro¹¹⁰, I.C. Arsene¹⁹, M. Arslanok¹³⁸, A. Augustinus³², R. Averbeck⁹⁷, M.D. Azmi¹⁵, H. Baba¹²⁴, A. Badalà⁵³, J. Bae¹⁰⁴, Y.W. Baek⁴⁰, X. Bai¹²⁰, R. Bailhache⁶⁴, Y. Bailung⁴⁸, R. Bala⁹¹, A. Balbino²⁹, A. Baldisseri¹³⁰, B. Balis², D. Banerjee⁴, Z. Banoo⁹¹, V. Barbasova³⁷, F. Barile³¹, L. Barioglio⁵⁶, M. Barlou⁷⁸, B. Barman⁴¹, G.G. Barnaföldi⁴⁶, L.S. Barnby¹¹⁵, E. Barreau¹⁰³, V. Barret¹²⁷, L. Barreto¹¹⁰, C. Bartels¹¹⁹, K. Barth³², E. Bartsch⁶⁴, N. Bastid¹²⁷, S. Basu⁷⁵, G. Batigne¹⁰³, D. Battistini⁹⁵, B. Batyunya¹⁴², D. Bauri⁴⁷, J.L. Bazo Alba¹⁰¹, I.G. Bearden⁸³, C. Beattie¹³⁸, P. Becht⁹⁷, D. Behera⁴⁸, I. Belikov¹²⁹, A.D.C. Bell Hechavarria¹²⁶, F. Bellini²⁵, R. Bellwied¹¹⁶, S. Belokurova¹⁴¹, L.G.E. Beltran¹⁰⁹, Y.A.V. Beltran⁴⁴, G. Bencedi⁴⁶, A. Bensaoula¹¹⁶, S. Beole²⁴, Y. Berdnikov¹⁴¹, A. Berdnikova⁹⁴, L. Bergmann⁹⁴, M.G. Besoiu⁶³, L. Betev³², P.P. Bhaduri¹³⁵, A. Bhasin⁹¹, B. Bhattacharjee⁴¹, L. Bianchi²⁴, N. Bianchi⁴⁹, J. Bielčik³⁵, J. Bielčiková⁸⁶, A.P. Bigot¹²⁹, A. Bilandzic⁹⁵, G. Biro⁴⁶, S. Biswas⁴, N. Bize¹⁰³, J.T. Blair¹⁰⁸, D. Blau¹⁴¹, M.B. Blidaru⁹⁷, N. Bluhme³⁸, C. Blume⁶⁴, G. Boca^{21,55}, F. Bock⁸⁷, T. Bodova²⁰, J. Bok¹⁶, L. Boldizsár⁴⁶, M. Bombara³⁷, P.M. Bond³², G. Bonomi^{134,55}, H. Borel¹³⁰, A. Borissov¹⁴¹, A.G. Borquez Carcamo⁹⁴, H. Bossi¹³⁸, E. Botta²⁴, Y.E.M. Bouziani⁶⁴, L. Bratrud⁶⁴, P. Braun-Munzinger⁹⁷, M. Bregant¹¹⁰, M. Broz³⁵, G.E. Bruno^{96,31}, V.D. Buchakchiev³⁶, M.D. Buckland²³, D. Budnikov¹⁴¹, H. Buesching⁶⁴, S. Bufalino²⁹, P. Buhler¹⁰², N. Burmasov¹⁴¹, Z. Buthelezi^{68,123}, A. Bylinkin²⁰, S.A. Bysiak¹⁰⁷, J.C. Cabanillas Noris¹⁰⁹, M.F.T. Cabrera¹¹⁶, M. Cai⁶, H. Caines¹³⁸, A. Caliva²⁸, E. Calvo Villar¹⁰¹, J.M.M. Camacho¹⁰⁹, P. Camerini²³, F.D.M. Canedo¹¹⁰, S.L. Cantway¹³⁸, M. Carabas¹¹³, A.A. Carballo³², F. Carnesecchi³², R. Caron¹²⁸, L.A.D. Carvalho¹¹⁰, J. Castillo Castellanos¹³⁰, M. Castoldi³², F. Catalano³², S. Cattaruzzi²³, C. Ceballos Sanchez¹⁴², R. Cerri²⁴, I. Chakaberia⁷⁴, P. Chakraborty^{136,47}, S. Chandra¹³⁵, S. Chapeland³², M. Chartier¹¹⁹, S. Chattopadhyay¹³⁵, S. Chattopadhyay¹³⁵, S. Chattopadhyay⁹⁹, M. Chen³⁹, T. Cheng^{97,6}, C. Cheshkov¹²⁸, V. Chibante Barroso³², D.D. Chinellato¹¹¹, E.S. Chizzali^{11,95}, J. Cho⁵⁸, S. Cho⁵⁸, P. Chochula³², Z.A. Chochulska¹³⁶, D. Choudhury⁴¹, P. Christakoglou⁸⁴, C.H. Christensen⁸³, P. Christiansen⁷⁵, T. Chujo¹²⁵, M. Ciaccio²⁹, C. Cicalo⁵², M.R. Ciupek⁹⁷, G. Clai^{III,51}, F. Colamaria⁵⁰, J.S. Colburn¹⁰⁰, D. Colella³¹, M. Colocci²⁵, M. Concas³², G. Conesa Balbastre⁷³, Z. Conesa del Valle¹³¹, G. Contin²³, J.G. Contreras³⁵, M.L. Coquet^{103,130}, P. Cortese^{133,56}, M.R. Cosentino¹¹², F. Costa³², S. Costanza^{21,55}, C. Cot¹³¹, J. Crkovská⁹⁴, P. Crochet¹²⁷, R. Cruz-Torres⁷⁴, P. Cui⁶, M.M. Czarnynoga¹³⁶, A. Dainese⁵⁴, G. Dange³⁸, M.C. Danisch⁹⁴, A. Danu⁶³, P. Das⁸⁰, P. Das⁴, S. Das⁴, A.R. Dash¹²⁶, S. Dash⁴⁷, A. De Caro²⁸, G. de Cataldo⁵⁰, J. de Cuveland³⁸, A. De Falco²², D. De Gruttola²⁸, N. De Marco⁵⁶, C. De Martin²³, S. De Pasquale²⁸, R. Deb¹³⁴, R. Del Grande⁹⁵, L. Dello Stritto³², W. Deng⁶, K.C. Devereaux¹⁸, P. Dhankher¹⁸, D. Di Bari³¹, A. Di Mauro³², B. Diab¹³⁰, R.A. Diaz^{142,7}, T. Dietel¹¹⁴, Y. Ding⁶, J. Ditzel⁶⁴, R. Divià³², Ø. Djuvsland²⁰, U. Dmitrieva¹⁴¹, A. Dobrin⁶³, B. Dönigus⁶⁴, J.M. Dubinski¹³⁶, A. Dubla⁹⁷, P. Dupieux¹²⁷, N. Dzalaiova¹³, T.M. Eder¹²⁶, R.J. Ehlers⁷⁴, F. Eisenhut⁶⁴, R. Ejima⁹², D. Elia⁵⁰, B. Erazmus¹⁰³, F. Ercolessi²⁵, B. Espagnon¹³¹, G. Eulisse³², D. Evans¹⁰⁰, S. Evdokimov¹⁴¹, L. Fabbietti⁹⁵, M. Faggin²³, J. Faivre⁷³, F. Fan⁶, W. Fan⁷⁴, A. Fantoni⁴⁹, M. Fasel⁸⁷, A. Feliciello⁵⁶, G. Feofilov¹⁴¹, A. Fernández Téllez⁴⁴, L. Ferrandi¹¹⁰, M.B. Ferrer³², A. Ferrero¹³⁰, C. Ferrero^{IV,56}, A. Ferretti²⁴, V.J.G. Feuillard⁹⁴, V. Filova³⁵, D. Finogeev¹⁴¹, F.M. Fionda⁵², E. Flatland³², F. Flor^{138,116}, A.N. Flores¹⁰⁸, S. Foertsch⁶⁸, I. Fokin⁹⁴, S. Fokin¹⁴¹, U. Follo^{IV,56}, E. Fragiaco⁵⁷, E. Frajna⁴⁶, U. Fuchs³², N. Funicello²⁸, C. Furget⁷³, A. Furs¹⁴¹, T. Fusayasu⁹⁸, J.J. Gaardhøje⁸³, M. Gagliardi²⁴, A.M. Gago¹⁰¹, T. Gahlaut⁴⁷, C.D. Galvan¹⁰⁹, D.R. Gangadharan¹¹⁶, P. Ganoti⁷⁸, C. Garabatos⁹⁷, J.M. García⁴⁴, T. García Chávez⁴⁴, E. Garcia-Solis⁹, C. Gargiulo³², P. Gasik⁹⁷, H.M. Gaur³⁸, A. Gautam¹¹⁸, M.B. Gay Ducati⁶⁶, M. Germain¹⁰³, C. Ghosh¹³⁵, M. Giacalone⁵¹, G. Gioachin²⁹, P. Giubellino^{97,56}, P. Giubileo²⁷, A.M.C. Glaenger¹³⁰, P. Glässel⁹⁴, E. Glimos¹²², D.J.Q. Goh⁷⁶, V. Gonzalez¹³⁷, P. Gordeev¹⁴¹, M. Gorgon², K. Goswami⁴⁸, S. Gotovac³³, V. Grabski⁶⁷, L.K. Graczykowski¹³⁶, E. Grecka⁸⁶, A. Grelli⁵⁹,

C. Grigoras³², V. Grigoriev¹⁴¹, S. Grigoryan^{142,1}, F. Grosa³², J.F. Grosse-Oetringhaus³², R. Grosso⁹⁷, D. Grund³⁵, N.A. Grunwald⁹⁴, G.G. Guardiano¹¹¹, R. Guernane⁷³, M. Guilbaud¹⁰³, K. Gulbrandsen⁸³, J.J.W.K. Gumprecht¹⁰², T. Gündem⁶⁴, T. Gunji¹²⁴, W. Guo⁶, A. Gupta⁹¹, R. Gupta⁹¹, R. Gupta⁴⁸, K. Gwizdziel¹³⁶, L. Gyulai⁴⁶, C. Hadjidakis¹³¹, F.U. Haider⁹¹, S. Haidlova³⁵, M. Haldar⁴, H. Hamagaki⁷⁶, A. Hamdi⁷⁴, Y. Han¹³⁹, B.G. Hanley¹³⁷, R. Hannigan¹⁰⁸, J. Hansen⁷⁵, M.R. Haque⁹⁷, J.W. Harris¹³⁸, A. Harton⁹, M.V. Hartung⁶⁴, H. Hassan¹¹⁷, D. Hatzifotiadou⁵¹, P. Hauer⁴², L.B. Havener¹³⁸, E. Hellbär⁹⁷, H. Helstrup³⁴, M. Hemmer⁶⁴, T. Herman³⁵, S.G. Hernandez¹¹⁶, G. Herrera Corral⁸, S. Herrmann¹²⁸, K.F. Hetland³⁴, B. Heybeck⁶⁴, H. Hillemanns³², B. Hippolyte¹²⁹, F.W. Hoffmann⁷⁰, B. Hofman⁵⁹, G.H. Hong¹³⁹, M. Horst⁹⁵, A. Horzyk², Y. Hou⁶, P. Hristov³², P. Huhn⁶⁴, L.M. Huhta¹¹⁷, T.J. Humanic⁸⁸, A. Hutson¹¹⁶, D. Hutter³⁸, M.C. Hwang¹⁸, R. Ilkaev¹⁴¹, M. Inaba¹²⁵, G.M. Innocenti³², M. Ippolitov¹⁴¹, A. Isakov⁸⁴, T. Isidori¹¹⁸, M.S. Islam⁹⁹, S. Iurchenko¹⁴¹, M. Ivanov⁹⁷, M. Ivanov¹³, V. Ivanov¹⁴¹, K.E. Iversen⁷⁵, M. Jablonski², B. Jacak^{18,74}, N. Jacazio²⁵, P.M. Jacobs⁷⁴, S. Jadlovská¹⁰⁶, J. Jadlovsky¹⁰⁶, S. Jaelani⁸², C. Jahnke¹¹⁰, M.J. Jakubowska¹³⁶, M.A. Janik¹³⁶, T. Janson⁷⁰, S. Ji¹⁶, S. Jia¹⁰, F. Jonas⁷⁴, D.M. Jones¹¹⁹, J.M. Jowett^{32,97}, J. Jung⁶⁴, M. Jung⁶⁴, A. Junique³², A. Jusko¹⁰⁰, J. Kaewjai¹⁰⁵, P. Kalinak⁶⁰, A. Kalweit³², A. Karasu Uysal⁷², D. Karatovic⁸⁹, N. Karatzenis¹⁰⁰, O. Karavichev¹⁴¹, T. Karavicheva¹⁴¹, E. Karpechev¹⁴¹, M.J. Karwowska^{32,136}, U. Keschull⁷⁰, R. Keidel¹⁴⁰, M. Keil³², B. Ketzer⁴², S.S. Khade⁴⁸, A.M. Khan¹²⁰, S. Khan¹⁵, A. Khanzadeev¹⁴¹, Y. Kharlov¹⁴¹, A. Khatun¹¹⁸, A. Khuntia³⁵, Z. Khuranova⁶⁴, B. Kileng³⁴, B. Kim¹⁰⁴, C. Kim¹⁶, D.J. Kim¹¹⁷, E.J. Kim⁶⁹, J. Kim¹³⁹, J. Kim⁵⁸, J. Kim^{32,69}, M. Kim¹⁸, S. Kim¹⁷, T. Kim¹³⁹, K. Kimura⁹², A. Kirkova³⁶, S. Kirsch⁶⁴, I. Kisel³⁸, S. Kiselev¹⁴¹, A. Kisiel¹³⁶, J.P. Kitowski², J.L. Klay⁵, J. Klein³², S. Klein⁷⁴, C. Klein-Bösing¹²⁶, M. Kleiner⁶⁴, T. Klemenz⁹⁵, A. Kluge³², C. Kobdaj¹⁰⁵, R. Kohara¹²⁴, T. Kollegger⁹⁷, A. Kondratyev¹⁴², N. Kondratyeva¹⁴¹, J. König⁶⁴, S.A. Königstorfer⁹⁵, P.J. Konopka³², G. Kornakov¹³⁶, M. Korwieser⁹⁵, S.D. Koryciak², C. Koster⁸⁴, A. Kotliarov⁸⁶, N. Kovacic⁸⁹, V. Kovalenko¹⁴¹, M. Kowalski¹⁰⁷, V. Kozuharov³⁶, I. Králik⁶⁰, A. Kravčáková³⁷, L. Krcal^{32,38}, M. Krivda^{100,60}, F. Krizek⁸⁶, K. Krizkova Gajdosova³², C. Krug⁶⁶, M. Krüger⁶⁴, D.M. Krupova³⁵, E. Kryshen¹⁴¹, V. Kučera⁵⁸, C. Kuhn¹²⁹, P.G. Kuijter⁸⁴, T. Kumaoka¹²⁵, D. Kumar¹³⁵, L. Kumar⁹⁰, N. Kumar⁹⁰, S. Kumar³¹, S. Kundu³², P. Kurashvili⁷⁹, A. Kurepin¹⁴¹, A.B. Kurepin¹⁴¹, A. Kuryakin¹⁴¹, S. Kushpil⁸⁶, V. Kuskov¹⁴¹, M. Kutyla¹³⁶, A. Kuznetsov¹⁴², M.J. Kweon⁵⁸, Y. Kwon¹³⁹, S.L. La Pointe³⁸, P. La Rocca²⁶, A. Lakrathok¹⁰⁵, M. Lamanna³², A.R. Landou⁷³, R. Langoy¹²¹, P. Larionov³², E. Laudi³², L. Lautner^{32,95}, R.A.N. Laveaga¹⁰⁹, R. Lavicka¹⁰², R. Lea^{134,55}, H. Lee¹⁰⁴, I. Legrand⁴⁵, G. Legras¹²⁶, J. Lehrbach³⁸, A.M. Lejeune³⁵, T.M. Lelek², R.C. Lemmon⁸⁵, I. León Monzón¹⁰⁹, M.M. Lesch⁹⁵, E.D. Lesser¹⁸, P. Lévai⁴⁶, M. Li⁶, X. Li¹⁰, B.E. Liang-gilman¹⁸, J. Lien¹²¹, R. Lietava¹⁰⁰, I. Likmeta¹¹⁶, B. Lim²⁴, S.H. Lim¹⁶, V. Lindenstruth³⁸, A. Lindner⁴⁵, C. Lippmann⁹⁷, D.H. Liu⁶, J. Liu¹¹⁹, G.S.S. Liveraro¹¹¹, I.M. Lofnes²⁰, C. Loizides⁸⁷, S. Lokos¹⁰⁷, J. Lömker⁵⁹, X. Lopez¹²⁷, E. López Torres⁷, P. Lu^{97,120}, F.V. Lugo⁶⁷, J.R. Luhder¹²⁶, M. Lunardon²⁷, G. Luparello⁵⁷, Y.G. Ma³⁹, M. Mager³², A. Maire¹²⁹, E.M. Majerz², M.V. Makariev³⁶, M. Malaev¹⁴¹, G. Malfattore²⁵, N.M. Malik⁹¹, Q.W. Malik¹⁹, S.K. Malik⁹¹, L. Malinina^{I,VIII,142}, D. Mallick¹³¹, N. Mallick⁴⁸, G. Mandaglio^{30,53}, S.K. Mandal⁷⁹, A. Manea⁶³, V. Manko¹⁴¹, F. Manso¹²⁷, V. Manzari⁵⁰, Y. Mao⁶, R.W. Marcjan², G.V. Margagliotti²³, A. Margotti⁵¹, A. Marín⁹⁷, C. Markert¹⁰⁸, P. Martinengo³², M.I. Martínez⁴⁴, G. Martínez García¹⁰³, M.P.P. Martins¹¹⁰, S. Masciocchi⁹⁷, M. Masera²⁴, A. Masoni⁵², L. Massacrier¹³¹, O. Massen⁵⁹, A. Mastroserio^{132,50}, O. Matonoha⁷⁵, S. Mattiazzo²⁷, A. Matyja¹⁰⁷, A.L. Mazuecos³², F. Mazzaschi^{32,24}, M. Mazzilli¹¹⁶, J.E. Mdhluli¹²³, Y. Melikyan⁴³, A. Menchaca-Rocha⁶⁷, J.E.M. Mendez⁶⁵, E. Meninno¹⁰², A.S. Menon¹¹⁶, M.W. Menzel^{32,94}, M. Meres¹³, Y. Miake¹²⁵, L. Micheletti³², D.L. Mihaylov⁹⁵, K. Mikhaylov^{142,141}, N. Minafra¹¹⁸, D. Miśkowiec⁹⁷, A. Modak^{134,4}, B. Mohanty⁸⁰, M. Mohisin Khan^{VI,15}, M.A. Molander⁴³, S. Monira¹³⁶, C. Mordasini¹¹⁷, D.A. Moreira De Godoy¹²⁶, I. Morozov¹⁴¹, A. Morsch³², T. Mrnjavac³², V. Muccifora⁴⁹, S. Muhuri¹³⁵, J.D. Mulligan⁷⁴, A. Mulliri²², M.G. Munhoz¹¹⁰, R.H. Munzer⁶⁴, H. Murakami¹²⁴, S. Murray¹¹⁴, L. Musa³², J. Musinsky⁶⁰, J.W. Myrcha¹³⁶, B. Naik¹²³, A.I. Nambrath¹⁸, B.K. Nandi⁴⁷, R. Nania⁵¹, E. Nappi⁵⁰, A.F. Nassirpour¹⁷, A. Nath⁹⁴, C. Nattrass¹²², M.N. Naydenov³⁶, A. Neagu¹⁹, A. Negru¹¹³, E. Nekrasova¹⁴¹, L. Nellen⁶⁵, R. Nepeivoda⁷⁵, S. Nese¹⁹, G. Neskovic³⁸, N. Nicassio⁵⁰, B.S. Nielsen⁸³, E.G. Nielsen⁸³, S. Nikolaev¹⁴¹, S. Nikulin¹⁴¹, V. Nikulin¹⁴¹, F. Noferini⁵¹, S. Noh¹², P. Nomokonov¹⁴², J. Norman¹¹⁹, N. Novitzky⁸⁷, P. Nowakowski¹³⁶, A. Nyanin¹⁴¹,

J. Nystrand²⁰, S. Oh¹⁷, A. Ohlson⁷⁵, V.A. Okorokov¹⁴¹, J. Oleniacz¹³⁶, A. Onnerstad¹¹⁷,
 C. Oppedisano⁵⁶, A. Ortiz Velasquez⁶⁵, J. Otwinowski¹⁰⁷, M. Oya⁹², K. Oyama⁷⁶, Y. Pachmayer⁹⁴,
 S. Padhan⁴⁷, D. Pagano^{134,55}, G. Paic⁶⁵, S. Paisano-Guzmán⁴⁴, A. Palasciano⁵⁰, S. Panebianco¹³⁰,
 H. Park¹²⁵, H. Park¹⁰⁴, J. Park¹²⁵, J.E. Parkkila³², Y. Patley⁴⁷, B. Paul²², M.M.D.M. Paulino¹¹⁰,
 H. Pei⁶, T. Peitzmann⁵⁹, X. Peng¹¹, M. Pennisi²⁴, S. Perciballi²⁴, D. Peresunko¹⁴¹, G.M. Perez⁷,
 Y. Pestov¹⁴¹, M.T. Petersen⁸³, V. Petrov¹⁴¹, M. Petrovici⁴⁵, S. Piano⁵⁷, M. Pikna¹³, P. Pillot¹⁰³,
 O. Pinazza^{51,32}, L. Pinsky¹¹⁶, C. Pinto⁹⁵, S. Pisano⁴⁹, M. Płoskoń⁷⁴, M. Planinic⁸⁹, F. Pliquett⁶⁴,
 M.G. Poghosyan⁸⁷, B. Polichtchouk¹⁴¹, S. Politano²⁹, N. Poljak⁸⁹, A. Pop⁴⁵,
 S. Porteboeuf-Houssais¹²⁷, V. Pozdniakov^{1,142}, I.Y. Pozos⁴⁴, K.K. Pradhan⁴⁸, S.K. Prasad⁴,
 S. Prasad⁴⁸, R. Preghenella⁵¹, F. Prino⁵⁶, C.A. Pruneau¹³⁷, I. Pshenichnov¹⁴¹, M. Puccio³²,
 S. Pucillo²⁴, S. Qiu⁸⁴, L. Quaglia²⁴, S. Ragoni¹⁴, A. Rai¹³⁸, A. Rakotozafindrabe¹³⁰,
 L. Ramello^{133,56}, F. Rami¹²⁹, M. Rasa²⁶, S.S. Räsänen⁴³, R. Rath⁵¹, M.P. Rauch²⁰,
 I. Ravasenga³², K.F. Read^{87,122}, C. Reckziegel¹¹², A.R. Redelbach³⁸, K. Redlich^{VII,79},
 C.A. Reetz⁹⁷, H.D. Regules-Medel⁴⁴, A. Rehman²⁰, F. Reidt³², H.A. Reme-Ness³⁴, Z. Rescakova³⁷,
 K. Reygers⁹⁴, A. Riabov¹⁴¹, V. Riabov¹⁴¹, R. Ricci²⁸, M. Richter²⁰, A.A. Riedel⁹⁵,
 W. Riegler³², A.G. Riffero²⁴, C. Ripoli²⁸, C. Ristea⁶³, M.V. Rodriguez³², M. Rodríguez Cahuantzi⁴⁴,
 S.A. Rodríguez Ramírez⁴⁴, K. Røed¹⁹, R. Rogalev¹⁴¹, E. Rogochaya¹⁴², T.S. Rogoschinski⁶⁴,
 D. Rohr³², D. Röhrich²⁰, S. Rojas Torres³⁵, P.S. Rokita¹³⁶, G. Romanenko²⁵, F. Ronchetti⁴⁹,
 E.D. Rosas⁶⁵, K. Roslon¹³⁶, A. Rossi⁵⁴, A. Roy⁴⁸, S. Roy⁴⁷, N. Rubini²⁵, J.A. Rudolph⁸⁴,
 D. Ruggiano¹³⁶, R. Rui²³, P.G. Russek², R. Russo⁸⁴, A. Rustamov⁸¹, E. Ryabinkin¹⁴¹,
 Y. Ryabov¹⁴¹, A. Rybicki¹⁰⁷, J. Ryu¹⁶, W. Rzeska¹³⁶, S. Sadhu³¹, S. Sadovsky¹⁴¹, J. Saetre²⁰,
 K. Šafařík³⁵, S.K. Saha⁴, S. Saha⁸⁰, B. Sahoo⁴⁸, R. Sahoo⁴⁸, S. Sahoo⁶¹, D. Sahu⁴⁸,
 P.K. Sahu⁶¹, J. Saini¹³⁵, K. Sajdakova³⁷, S. Sakai¹²⁵, M.P. Salvan⁹⁷, S. Sambyal⁹¹, D. Samitz¹⁰²,
 I. Sanna^{32,95}, T.B. Saramela¹¹⁰, D. Sarkar⁸³, P. Sarma⁴¹, V. Sarritzu²², V.M. Sarti⁹⁵, M.H.P. Sas³²,
 S. Sawan⁸⁰, E. Scapparone⁵¹, J. Schambach⁸⁷, H.S. Scheid⁶⁴, C. Schiaua⁴⁵, R. Schicker⁹⁴,
 F. Schlegler⁹⁴, A. Schmah⁹⁷, C. Schmidt⁹⁷, H.R. Schmidt⁹³, M.O. Schmidt³², M. Schmidt⁹³,
 N.V. Schmidt⁸⁷, A.R. Schmier¹²², R. Schotter¹²⁹, A. Schröter³⁸, J. Schukraft³², K. Schweda⁹⁷,
 G. Scioli²⁵, E. Scomparin⁵⁶, J.E. Seger¹⁴, Y. Sekiguchi¹²⁴, D. Sekihata¹²⁴, M. Selina⁸⁴,
 I. Selyuzhenkov⁹⁷, S. Senyukov¹²⁹, J.J. Seo⁹⁴, D. Serebryakov¹⁴¹, L. Serkin⁶⁵, L. Šerkšnytė⁹⁵,
 A. Sevcenco⁶³, T.J. Shaba⁶⁸, A. Shabetai¹⁰³, R. Shahoyan³², A. Shangaraev¹⁴¹, B. Sharma⁹¹,
 D. Sharma⁴⁷, H. Sharma⁵⁴, M. Sharma⁹¹, S. Sharma⁷⁶, S. Sharma⁹¹, U. Sharma⁹¹, A. Shatat¹³¹,
 O. Sheibani¹¹⁶, K. Shigaki⁹², M. Shimomura⁷⁷, J. Shin¹², S. Shirinkin¹⁴¹, Q. Shou³⁹, Y. Sibiriak¹⁴¹,
 S. Siddhanta⁵², T. Siemiarczuk⁷⁹, T.F. Silva¹¹⁰, D. Silvermyr⁷⁵, T. Simantathammakul¹⁰⁵,
 R. Simeonov³⁶, B. Singh⁹¹, B. Singh⁹⁵, K. Singh⁴⁸, R. Singh⁸⁰, R. Singh⁹¹, R. Singh^{97,48},
 S. Singh¹⁵, V.K. Singh¹³⁵, V. Singhal¹³⁵, T. Sinha⁹⁹, B. Sitar¹³, M. Sitta^{133,56}, T.B. Skaali¹⁹,
 G. Skorodumovs⁹⁴, N. Smirnov¹³⁸, R.J.M. Snellings⁵⁹, E.H. Solheim¹⁹, J. Song¹⁶,
 C. Sonnabend^{32,97}, J.M. Sonneveld⁸⁴, F. Soramel²⁷, A.B. Soto-hernandez⁸⁸, R. Spijkers⁸⁴,
 I. Sputowska¹⁰⁷, J. Staa⁷⁵, J. Stachel⁹⁴, I. Stan⁶³, P.J. Steffanic¹²², S.F. Stiefelmaier⁹⁴,
 D. Stocco¹⁰³, I. Storehaug¹⁹, N.J. Strangmann⁶⁴, P. Stratmann¹²⁶, S. Strazzi²⁵, A. Sturmiolo^{30,53},
 C.P. Stylianidis⁸⁴, A.A.P. Suaide¹¹⁰, C. Suires¹³¹, M. Sukhanov¹⁴¹, M. Suljic³², R. Sultanov¹⁴¹,
 V. Sumberia⁹¹, S. Sumowidagdo⁸², I. Szarka¹³, M. Szymkowski¹³⁶, S.F. Taghavi⁹⁵,
 G. Taillepied⁹⁷, J. Takahashi¹¹¹, G.J. Tambave⁸⁰, S. Tang⁶, Z. Tang¹²⁰, J.D. Tapia Takaki¹¹⁸,
 N. Tapus¹¹³, L.A. Tarasovicova¹²⁶, M.G. Tazila⁴⁵, G.F. Tassielli³¹, A. Tauro³², A. Tavira García¹³¹,
 G. Tejeda Muñoz⁴⁴, A. Telesca³², L. Terlizzi²⁴, C. Terrevoli⁵⁰, S. Thakur⁴, D. Thomas¹⁰⁸,
 A. Tikhonov¹⁴¹, N. Tiltmann^{32,126}, A.R. Timmins¹¹⁶, M. Tkacik¹⁰⁶, T. Tkacik¹⁰⁶, A. Toia⁶⁴,
 R. Tokumoto⁹², S. Tomassini²⁵, K. Tomohiro⁹², N. Topilskaya¹⁴¹, M. Toppi⁴⁹, T. Tork¹³¹,
 V.V. Torres¹⁰³, A.G. Torres Ramos³¹, A. Trifiro^{30,53}, T. Triloki⁹⁶, A.S. Triolo^{32,30,53}, S. Tripathy³²,
 T. Tripathy⁴⁷, V. Trubnikov³, W.H. Trzaska¹¹⁷, T.P. Trzcinski¹³⁶, C. Tsolanta¹⁹, R. Tu³⁹,
 A. Tumkin¹⁴¹, R. Turrisi⁵⁴, T.S. Tveter¹⁹, K. Ullaland²⁰, B. Ulukutlu⁹⁵, A. Uras¹²⁸,
 M. Urioni¹³⁴, G.L. Usai²², M. Vala³⁷, N. Valle⁵⁵, L.V.R. van Doremalen⁵⁹, M. van Leeuwen⁸⁴,
 C.A. van Veen⁹⁴, R.J.G. van Weelden⁸⁴, P. Vande Vyvre³², D. Varga⁴⁶, Z. Varga⁴⁶,
 P. Vargas Torres⁶⁵, M. Vasileiou⁷⁸, A. Vasiliev¹⁴¹, O. Vázquez Doce⁴⁹, O. Vazquez Rueda¹¹⁶,
 V. Vechernin¹⁴¹, E. Vercellin²⁴, S. Vergara Limón⁴⁴, R. Verma⁴⁷, L. Vermunt⁹⁷, R. Vértesi⁴⁶,
 M. Verweij⁵⁹, L. Vickovic³³, Z. Vilakazi¹²³, O. Villalobos Baillie¹⁰⁰, A. Villani²³, A. Vinogradov¹⁴¹,
 T. Virgili²⁸, M.M.O. Virta¹¹⁷, V. Vislavicius⁷⁵, A. Vodopyanov¹⁴², B. Volkel³², M.A. Völkl⁹⁴,
 S.A. Voloshin¹³⁷, G. Volpe³¹, B. von Haller³², I. Vorobyev³², N. Vozniuk¹⁴¹, J. Vrláková³⁷,

J. Wan³⁹, C. Wang³⁹, D. Wang³⁹, Y. Wang³⁹, Y. Wang⁶, A. Wegrzynek³², F.T. Weiglhofer³⁸, S.C. Wenzel³², J.P. Wessels¹²⁶, J. Wiechula⁶⁴, J. Wikne¹⁹, G. Wilk⁷⁹, J. Wilkinson⁹⁷, G.A. Willems¹²⁶, B. Windelband⁹⁴, M. Winn¹³⁰, J.R. Wright¹⁰⁸, W. Wu³⁹, Y. Wu¹²⁰, Z. Xiong¹²⁰, R. Xu⁶, A. Yadav⁴², A.K. Yadav¹³⁵, Y. Yamaguchi⁹², S. Yang²⁰, S. Yano⁹², E.R. Yeats¹⁸, Z. Yin⁶, I.-K. Yoo¹⁶, J.H. Yoon⁵⁸, H. Yu¹², S. Yuan²⁰, A. Yuncu⁹⁴, V. Zaccolo²³, C. Zampolli³², M. Zang⁶, F. Zanone⁹⁴, N. Zardoshti³², A. Zarochentsev¹⁴¹, P. Závada⁶², N. Zaviyalov¹⁴¹, M. Zhalov¹⁴¹, B. Zhang⁶, C. Zhang¹³⁰, L. Zhang³⁹, M. Zhang^{127,6}, S. Zhang³⁹, X. Zhang⁶, Y. Zhang¹²⁰, Z. Zhang⁶, M. Zhao¹⁰, V. Zhrebchevskii¹⁴¹, Y. Zhi¹⁰, D. Zhou⁶, Y. Zhou⁸³, J. Zhu^{54,6}, S. Zhu¹²⁰, Y. Zhu⁶, S.C. Zugravel⁵⁶, N. Zurlo^{134,55}

Affiliation Notes

^I Deceased

^{II} Also at: Max-Planck-Institut für Physik, Munich, Germany

^{III} Also at: Italian National Agency for New Technologies, Energy and Sustainable Economic Development (ENEA), Bologna, Italy

^{IV} Also at: Dipartimento DET del Politecnico di Torino, Turin, Italy

^V Also at: Yildiz Technical University, Istanbul, Türkiye

^{VI} Also at: Department of Applied Physics, Aligarh Muslim University, Aligarh, India

^{VII} Also at: Institute of Theoretical Physics, University of Wrocław, Poland

^{VIII} Also at: An institution covered by a cooperation agreement with CERN

Collaboration Institutes

¹ A.I. Alikhanyan National Science Laboratory (Yerevan Physics Institute) Foundation, Yerevan, Armenia

² AGH University of Krakow, Cracow, Poland

³ Bogolyubov Institute for Theoretical Physics, National Academy of Sciences of Ukraine, Kiev, Ukraine

⁴ Bose Institute, Department of Physics and Centre for Astroparticle Physics and Space Science (CAPSS), Kolkata, India

⁵ California Polytechnic State University, San Luis Obispo, California, United States

⁶ Central China Normal University, Wuhan, China

⁷ Centro de Aplicaciones Tecnológicas y Desarrollo Nuclear (CEADEN), Havana, Cuba

⁸ Centro de Investigación y de Estudios Avanzados (CINVESTAV), Mexico City and Mérida, Mexico

⁹ Chicago State University, Chicago, Illinois, United States

¹⁰ China Institute of Atomic Energy, Beijing, China

¹¹ China University of Geosciences, Wuhan, China

¹² Chungbuk National University, Cheongju, Republic of Korea

¹³ Comenius University Bratislava, Faculty of Mathematics, Physics and Informatics, Bratislava, Slovak Republic

¹⁴ Creighton University, Omaha, Nebraska, United States

¹⁵ Department of Physics, Aligarh Muslim University, Aligarh, India

¹⁶ Department of Physics, Pusan National University, Pusan, Republic of Korea

¹⁷ Department of Physics, Sejong University, Seoul, Republic of Korea

¹⁸ Department of Physics, University of California, Berkeley, California, United States

¹⁹ Department of Physics, University of Oslo, Oslo, Norway

²⁰ Department of Physics and Technology, University of Bergen, Bergen, Norway

²¹ Dipartimento di Fisica, Università di Pavia, Pavia, Italy

²² Dipartimento di Fisica dell'Università and Sezione INFN, Cagliari, Italy

²³ Dipartimento di Fisica dell'Università and Sezione INFN, Trieste, Italy

²⁴ Dipartimento di Fisica dell'Università and Sezione INFN, Turin, Italy

²⁵ Dipartimento di Fisica e Astronomia dell'Università and Sezione INFN, Bologna, Italy

²⁶ Dipartimento di Fisica e Astronomia dell'Università and Sezione INFN, Catania, Italy

²⁷ Dipartimento di Fisica e Astronomia dell'Università and Sezione INFN, Padova, Italy

²⁸ Dipartimento di Fisica 'E.R. Caianiello' dell'Università and Gruppo Collegato INFN, Salerno, Italy

²⁹ Dipartimento DISAT del Politecnico and Sezione INFN, Turin, Italy

³⁰ Dipartimento di Scienze MIFT, Università di Messina, Messina, Italy

³¹ Dipartimento Interateneo di Fisica 'M. Merlin' and Sezione INFN, Bari, Italy

- ³² European Organization for Nuclear Research (CERN), Geneva, Switzerland
- ³³ Faculty of Electrical Engineering, Mechanical Engineering and Naval Architecture, University of Split, Split, Croatia
- ³⁴ Faculty of Engineering and Science, Western Norway University of Applied Sciences, Bergen, Norway
- ³⁵ Faculty of Nuclear Sciences and Physical Engineering, Czech Technical University in Prague, Prague, Czech Republic
- ³⁶ Faculty of Physics, Sofia University, Sofia, Bulgaria
- ³⁷ Faculty of Science, P.J. Šafárik University, Košice, Slovak Republic
- ³⁸ Frankfurt Institute for Advanced Studies, Johann Wolfgang Goethe-Universität Frankfurt, Frankfurt, Germany
- ³⁹ Fudan University, Shanghai, China
- ⁴⁰ Gangneung-Wonju National University, Gangneung, Republic of Korea
- ⁴¹ Gauhati University, Department of Physics, Guwahati, India
- ⁴² Helmholtz-Institut für Strahlen- und Kernphysik, Rheinische Friedrich-Wilhelms-Universität Bonn, Bonn, Germany
- ⁴³ Helsinki Institute of Physics (HIP), Helsinki, Finland
- ⁴⁴ High Energy Physics Group, Universidad Autónoma de Puebla, Puebla, Mexico
- ⁴⁵ Horia Hulubei National Institute of Physics and Nuclear Engineering, Bucharest, Romania
- ⁴⁶ HUN-REN Wigner Research Centre for Physics, Budapest, Hungary
- ⁴⁷ Indian Institute of Technology Bombay (IIT), Mumbai, India
- ⁴⁸ Indian Institute of Technology Indore, Indore, India
- ⁴⁹ INFN, Laboratori Nazionali di Frascati, Frascati, Italy
- ⁵⁰ INFN, Sezione di Bari, Bari, Italy
- ⁵¹ INFN, Sezione di Bologna, Bologna, Italy
- ⁵² INFN, Sezione di Cagliari, Cagliari, Italy
- ⁵³ INFN, Sezione di Catania, Catania, Italy
- ⁵⁴ INFN, Sezione di Padova, Padova, Italy
- ⁵⁵ INFN, Sezione di Pavia, Pavia, Italy
- ⁵⁶ INFN, Sezione di Torino, Turin, Italy
- ⁵⁷ INFN, Sezione di Trieste, Trieste, Italy
- ⁵⁸ Inha University, Incheon, Republic of Korea
- ⁵⁹ Institute for Gravitational and Subatomic Physics (GRASP), Utrecht University/Nikhef, Utrecht, Netherlands
- ⁶⁰ Institute of Experimental Physics, Slovak Academy of Sciences, Košice, Slovak Republic
- ⁶¹ Institute of Physics, Homi Bhabha National Institute, Bhubaneswar, India
- ⁶² Institute of Physics of the Czech Academy of Sciences, Prague, Czech Republic
- ⁶³ Institute of Space Science (ISS), Bucharest, Romania
- ⁶⁴ Institut für Kernphysik, Johann Wolfgang Goethe-Universität Frankfurt, Frankfurt, Germany
- ⁶⁵ Instituto de Ciencias Nucleares, Universidad Nacional Autónoma de México, Mexico City, Mexico
- ⁶⁶ Instituto de Física, Universidade Federal do Rio Grande do Sul (UFRGS), Porto Alegre, Brazil
- ⁶⁷ Instituto de Física, Universidad Nacional Autónoma de México, Mexico City, Mexico
- ⁶⁸ iThemba LABS, National Research Foundation, Somerset West, South Africa
- ⁶⁹ Jeonbuk National University, Jeonju, Republic of Korea
- ⁷⁰ Johann-Wolfgang-Goethe Universität Frankfurt Institut für Informatik, Fachbereich Informatik und Mathematik, Frankfurt, Germany
- ⁷¹ Korea Institute of Science and Technology Information, Daejeon, Republic of Korea
- ⁷² KTO Karatay University, Konya, Turkey
- ⁷³ Laboratoire de Physique Subatomique et de Cosmologie, Université Grenoble-Alpes, CNRS-IN2P3, Grenoble, France
- ⁷⁴ Lawrence Berkeley National Laboratory, Berkeley, California, United States
- ⁷⁵ Lund University Department of Physics, Division of Particle Physics, Lund, Sweden
- ⁷⁶ Nagasaki Institute of Applied Science, Nagasaki, Japan
- ⁷⁷ Nara Women's University (NWU), Nara, Japan
- ⁷⁸ National and Kapodistrian University of Athens, School of Science, Department of Physics, Athens, Greece
- ⁷⁹ National Centre for Nuclear Research, Warsaw, Poland
- ⁸⁰ National Institute of Science Education and Research, Homi Bhabha National Institute, Jatni, India
- ⁸¹ National Nuclear Research Center, Baku, Azerbaijan
- ⁸² National Research and Innovation Agency - BRIN, Jakarta, Indonesia

- ⁸³ Niels Bohr Institute, University of Copenhagen, Copenhagen, Denmark
⁸⁴ Nikhef, National institute for subatomic physics, Amsterdam, Netherlands
⁸⁵ Nuclear Physics Group, STFC Daresbury Laboratory, Daresbury, United Kingdom
⁸⁶ Nuclear Physics Institute of the Czech Academy of Sciences, Husinec-Řež, Czech Republic
⁸⁷ Oak Ridge National Laboratory, Oak Ridge, Tennessee, United States
⁸⁸ Ohio State University, Columbus, Ohio, United States
⁸⁹ Physics department, Faculty of science, University of Zagreb, Zagreb, Croatia
⁹⁰ Physics Department, Panjab University, Chandigarh, India
⁹¹ Physics Department, University of Jammu, Jammu, India
⁹² Physics Program and International Institute for Sustainability with Knotted Chiral Meta Matter (SKCM2), Hiroshima University, Hiroshima, Japan
⁹³ Physikalisches Institut, Eberhard-Karls-Universität Tübingen, Tübingen, Germany
⁹⁴ Physikalisches Institut, Ruprecht-Karls-Universität Heidelberg, Heidelberg, Germany
⁹⁵ Physik Department, Technische Universität München, Munich, Germany
⁹⁶ Politecnico di Bari and Sezione INFN, Bari, Italy
⁹⁷ Research Division and ExtreMe Matter Institute EMMI, GSI Helmholtzzentrum für Schwerionenforschung GmbH, Darmstadt, Germany
⁹⁸ Saga University, Saga, Japan
⁹⁹ Saha Institute of Nuclear Physics, Homi Bhabha National Institute, Kolkata, India
¹⁰⁰ School of Physics and Astronomy, University of Birmingham, Birmingham, United Kingdom
¹⁰¹ Sección Física, Departamento de Ciencias, Pontificia Universidad Católica del Perú, Lima, Peru
¹⁰² Stefan Meyer Institut für Subatomare Physik (SMI), Vienna, Austria
¹⁰³ SUBATECH, IMT Atlantique, Nantes Université, CNRS-IN2P3, Nantes, France
¹⁰⁴ Sungkyunkwan University, Suwon City, Republic of Korea
¹⁰⁵ Suranaree University of Technology, Nakhon Ratchasima, Thailand
¹⁰⁶ Technical University of Košice, Košice, Slovak Republic
¹⁰⁷ The Henryk Niewodniczanski Institute of Nuclear Physics, Polish Academy of Sciences, Cracow, Poland
¹⁰⁸ The University of Texas at Austin, Austin, Texas, United States
¹⁰⁹ Universidad Autónoma de Sinaloa, Culiacán, Mexico
¹¹⁰ Universidade de São Paulo (USP), São Paulo, Brazil
¹¹¹ Universidade Estadual de Campinas (UNICAMP), Campinas, Brazil
¹¹² Universidade Federal do ABC, Santo Andre, Brazil
¹¹³ Universitatea Nationala de Stiinta si Tehnologie Politehnica Bucuresti, Bucharest, Romania
¹¹⁴ University of Cape Town, Cape Town, South Africa
¹¹⁵ University of Derby, Derby, United Kingdom
¹¹⁶ University of Houston, Houston, Texas, United States
¹¹⁷ University of Jyväskylä, Jyväskylä, Finland
¹¹⁸ University of Kansas, Lawrence, Kansas, United States
¹¹⁹ University of Liverpool, Liverpool, United Kingdom
¹²⁰ University of Science and Technology of China, Hefei, China
¹²¹ University of South-Eastern Norway, Kongsberg, Norway
¹²² University of Tennessee, Knoxville, Tennessee, United States
¹²³ University of the Witwatersrand, Johannesburg, South Africa
¹²⁴ University of Tokyo, Tokyo, Japan
¹²⁵ University of Tsukuba, Tsukuba, Japan
¹²⁶ Universität Münster, Institut für Kernphysik, Münster, Germany
¹²⁷ Université Clermont Auvergne, CNRS/IN2P3, LPC, Clermont-Ferrand, France
¹²⁸ Université de Lyon, CNRS/IN2P3, Institut de Physique des 2 Infinis de Lyon, Lyon, France
¹²⁹ Université de Strasbourg, CNRS, IPHC UMR 7178, F-67000 Strasbourg, France, Strasbourg, France
¹³⁰ Université Paris-Saclay, Centre d'Etudes de Saclay (CEA), IRFU, Département de Physique Nucléaire (DPhN), Saclay, France
¹³¹ Université Paris-Saclay, CNRS/IN2P3, IJCLab, Orsay, France
¹³² Università degli Studi di Foggia, Foggia, Italy
¹³³ Università del Piemonte Orientale, Vercelli, Italy
¹³⁴ Università di Brescia, Brescia, Italy
¹³⁵ Variable Energy Cyclotron Centre, Homi Bhabha National Institute, Kolkata, India

¹³⁶ Warsaw University of Technology, Warsaw, Poland

¹³⁷ Wayne State University, Detroit, Michigan, United States

¹³⁸ Yale University, New Haven, Connecticut, United States

¹³⁹ Yonsei University, Seoul, Republic of Korea

¹⁴⁰ Zentrum für Technologie und Transfer (ZTT), Worms, Germany

¹⁴¹ Affiliated with an institute covered by a cooperation agreement with CERN

¹⁴² Affiliated with an international laboratory covered by a cooperation agreement with CERN.